SUBCRITICAL TRANSMUTATION OF SPENT NUCLEAR FUEL

A Thesis
Presented to
The Academic Faculty

by

Christopher M. Sommer

In Partial Fulfillment
of the Requirements for the Degree
Doctor of Philosophy in
Nuclear Engineering

Nuclear and Radiological Engineering
Georgia Institute of Technology
August 2011

SUBCRITICAL TRANSMUTATION OF SPENT NUCLEAR FUEL

Approved by:

Dr. Weston Stacey, Advisor
Nuclear and Radiological Engineering
Georgia Institute of Technology

Dr. Farzad Rahnema
Department of Nuclear and
Radiological Engineering
Georgia Institute of Technology

Dr. Bojan Petrovic
Department of Nuclear and
Radiological Engineering
Georgia Institute of Technology

Dr. Adam Stulberg
Department of International Affairs
Georgia Institute of Technology

Dr. Nolan Hertel
Department of Nuclear and
Radiological Engineering
Georgia Institute of Technology

Dr. Ed Hoffman
Nuclear Engineering Division
Argonne National Laboratory

Date Approved: July, 6th 2011

ACKNOWLEDGEMENTS

I want to thank my advisor, Dr. Stacey, for all his help and advice throughout the project and all of my graduate studies at Georgia Tech. I would also like to thank the other members of my committee, Dr. Petrovic, Dr. Rahnema, Dr. Hertel, and Dr. Stulberg from Georgia Tech, and Dr. Hoffman from ANL. I want to send a special thanks to Dr. van Rooijen for his help at the beginning of my graduate studies as well as on the beginning stages of this research. I would like to thank all of my fellow students in the fast reactor research group as well as the fusion research center for helping me throughout the project. A great amount of gratitude to Tyler Sumner who has probably helped me more than he knows by listening to my rants over the past four years. I want to thank my parents for always being there for me and their encouragement along this journey. Finally and most importantly I want to thank my wife for understanding all of the late nights and her love and support along the way.

TABLE OF CONTENTS

ACKNOWLEDGEMENTS . . . . . **iii**

LIST OF TABLES . . . . . **vi**

LIST OF FIGURES . . . . . **vii**

SUMMARY . . . . . **ix**

I INTRODUCTION **1**

II BACKGROUND **4**

2.1 Advantages of Subcritical Transmutation 4

2.2 Advantages of Fusion-Fission Hybrid Reactors 5

2.3 Evolution of Subcritical Advanced Burner Reactor (SABR) 6

2.3.1 SABR Design 6

2.4 Reprocessing 20

2.4.1 Aqueous Reprocessing 20

2.4.2 Electrochemical Reprocessing 21

III SABR FUEL CYCLE **23**

3.1 SABR Fuel Cycle 23

IV COMPUTATIONAL TOOLS **25**

4.1 ERANOS2.0 25

4.2 ORIGEN-S 27

4.3 Computational Model 28

V FUEL CYCLE SIMULATIONS **30**

5.1 Accumulated Radiation Damage versus Burnup 33

5.1.1 Power Distribution for the Accumulated Radiation vs Burnup Fuel Cycles 35

5.1.2 Repository Effects of the the Accumulated Radiation vs Burnup Fuel Cycles 36

5.2 TRU Burner Fuel Cycle 39
5.2.1 Radiation Damage Benefits of Fuel Rotation 39
5.2.2 Power Profiles for the 200 dpa Rotated TRU Burner Fuel Cycle 44
5.2.3 Repository Effects for the Rotated and Non-Rotated TRU Burner Fuel Cycle 50
5.2.4 Tritium Breeding Gain for the Rotated 200 dpa TRU Burner Fuel Cycle 52
5.3 Minor Actinide Burner 58
5.3.1 Radiation Damage in the Metallic and Oxide Minor Actinide Burning Fuel Cycles 61
5.3.2 Power Profiles for the Metallic and Oxide Minor Actinide Burning Fuel Cycles 67
5.3.3 Repository Effects of the Metallic and Oxide Minor Actinide Burning Fuel Cycle 70
5.3.4 Tritium Breeding in the Metallic and Oxide Minor Actinide Burning Fuel Cycles 74
5.4 SABR Fuel Cycle Comparisons 75
5.4.1 TRU Burning Fuel Cycle 77
5.4.2 Comparison of SABR Minor Actinide Burning Fuel Cycles to EFIT and LCRFR Fuel Cycles 79
VI CONCLUSIONS **81**
REFERENCES **85**

LIST OF TABLES

1 ANL Fuel BOL TRU Composition [29] 8

2 Minor Actinide Burning Fuel Vector for the Minor Actinide Burning Fuel [12] 11

3 Key Design Parameters for the SABR Metal and Oxide Fuel Pin and Assembly 14

4 Major Parameters for the Fission Core in SABR [38] 18

5 Major Parameters for the Fusion Neutron Source in SABR [35] . . . 19

6 Recovery Efficiency of Key Elements in UREX Process [15] 21

7 Accumulated Radiation Damage versus Burnup Fuel Cycle Results . . 34

8 Recovery Efficiency of Key Elements for Electrochemical Reprocessing [30] 36

9 Transuranic Waste in Kilograms to the Repository after each Reprocessing Step for SABR 37

10 Tritium Production for the 200 dpa TRU Burner Fuel Cycle 53

11 TRU Burner 200 dpa Rotated and Non-Rotated Fuel Cycle Results . 54

12 SABR Fuel Compositions at BOC and EOC for the TRU Burning Fuel Cycles (weight percent) 56

13 SABR Content to the Repository and Fuel Fabrication for the MA Burning Fuel Cycles (kg) 57

14 MA Burner Metallic and Oxide Fuel Cycle Results 59

15 SABR Fuel Compositions at BOC and EOC for the MA Burning Fuel Cycles (weight percent) 71

16 SABR Content to the Repository and Fuel Fabrication for the MA burning Fuel Cycles (kg) 72

17 Tritium Production for the MA Burning Fuel Cycles 75

18 System Data for SABR Equilibrium Fuel Cycle 77

19 Transmutation Capabilities of SABR, EFIT, and LCRFR 78

LIST OF FIGURES

1 Multi Strata Transmutation Fuel Cycle [2] 2

2 Three Dimensional Schematic for SABR 7

3 Axial View of SABR Fuel Pin 9

4 Cross-Section of Metallic ANL-Fuel Pin 9

5 Cross-Section of SABR Metallic Fuel Assembly 10

6 Cross-Section of SABR MA-Oxide Fuel Pin 12

7 Cross-Section of SABR MA-Oxide Fuel Assembly 13

8 Lithium (n, α) Cross Section Comparison 15

9 In to Out Shuffling Pattern for the SABR Fuel Cycle 24

10 SABR RZ Computational Model used in ERANOS2.0 28

11 Ratio of Am^{241} Fission Cross Section to Pu^{239} Fission Cross Section . 31

12 Transmutation and Separation Methods to Increase the Effective Space of Yucca Mountain [32] 32

13 Radial Power Distribution for the TRU Burner Fuel Cycles 35

14 Comparison of Decay Heat to the Repository for Different Fuel Cycle Lengths 38

15 Radiation Damage by Region for the 200 dpa TRU Burner Fuel Cycle 40

16 Flux Spectrum by Ring for the 200 dpa TRU Burner Fuel Cycle . . . 41

17 Radiation Damage Production as a Function of Energy, for the 200 dpa TRU Burner Fuel Cycle 42

18 Rotation Pattern for SABR Fuel Cycle 43

19 Accumulated Radiation Damage versus Region for the 200 dpa TRU Burner Fuel Cycle 44

20 Power Distribution for 200 dpa TRU Burner Fuel Cycle 45

21 Power Density per Half Assembly for the 200 dpa TRU Burner Fuel Cycle 46

22 Flux Spectrum by Ring for the 200 dpa TRU burner Fuel Cycle without the Inner Tritium Breeding Blanket 47

23 Radial Power Distribution Comparison for the 200 dpa TRU Burner Fuel Cycle with and without the Inner Tritium Breeding Blanket . . . 47

24 Fission Power Produced by Neutrons in Different Energy Ranges for the 200 dpa TRU Burner Fuel Cycle without the Inner Tritium Breeding Blanket 200 48

25 Fission Power Produced by Neutrons in Different Energy Ranges for the 200 dpa TRU Burner Fuel Cycle 48

26 Axial Power Profile in each Assembly Region for the 200 dpa TRU Burner Fuel Cycle 50

27 Decay heat to the repository for the Rotated and Non-Rotated 200 dpa Fuel Cycle 51

28 Normalized Neutron Flux Spectrum for the Minor Actinide Oxide and Metallic Fuel 61

29 Radiation Damage by region for the Minor Actinide Burning Fuel Cycles 62

30 Accumulated Radiation Damage by Region for the Metallic and Oxide Fuel Cycles 63

31 Neutron Spectra by Ring for the MA-Oxide Fuel Cycle 64

32 Neutron Spectra by Ring for the MA-Metal Fuel Cycle 64

33 MA-Oxide Radiation Damage Production as a Function of Space and Energy 65

34 MA-Metal Radiation Damage Production as a Function of Space and Energy 66

35 Radial Power Distributions for MA-Metal and MA-Oxide Fuel Cycles 67

36 Power per Half Assembly for MA-Metal and MA-Oxide Fuel Cycles . 68

37 Axial Power Profile for the MA-Oxide Fuel Cycle 69

38 Axial Power Profile for the MA-Metal Fuel Cycle 69

39 Decay Heat to the Repository MA-Oxide and MA-Metal Fuel Cycles 74

SUMMARY

A series of fuel cycle simulations were performed using CEA's reactor physics code ERANOS 2.0 to analyze the transmutation performance of the Subcritical Advanced Burner Reactor (SABR). SABR is a fusion-fission hybrid reactor that combines the leading sodium cooled fast reactor technology with the leading tokamak plasma technology based on ITER physics. Two general fuel cycles were considered for the SABR system. The first fuel cycle is one in which all of the transuranics from light water reactors are burned in SABR. The second fuel cycle is a minor actinide burning fuel cycle in which all of the minor actinides and some of the plutonium produced in light water reactors are burned in SABR, with the excess plutonium being set aside for starting up fast reactors in the future. The minor actinide burning fuel cycle is being considered in European Scenario Studies. The fuel cycles were evaluated on the basis of TRU/MA transmutation rate, power profile, accumulated radiation damage, and decay heat to the repository. Each of the fuel cycles are compared against each other, and the minor actinide burning fuel cycles are compared against the EFIT transmutation system, and a low conversion ratio fast reactor.

CHAPTER I

INTRODUCTION

The forecast for increased power generation through nuclear power in the next 30 years exacerbates the issue of spent nuclear fuel disposal. Between 2007 and 2010 the Nuclear Regulatory Commission (NRC) has accepted applications for 26 new light water reactors and expects applications for another 5 reactors in 2011 [4]. These 31 reactors would increase the current nuclear power output of the U.S by approximately 30%, increasing the amount of discharge fuel needed to be stored in geological repositories by a comparable amount.

One option for disposal of spent nuclear fuel (SNF) is initial on site storage followed by shipping of the fuel to a geological repository where it can be permanently interned. At today's rate of power generation enough spent fuel will be created to fill a Yucca Mountain type repository by the year 2020 [28]. With the predicted increase in nuclear power a new geological repository of the same capacity as Yucca Mountain would be needed every 45 years.

A second option for spent fuel disposal is to introduce a multi strata fuel cycle in which the actinides in the spent fuel from light water reactors (LWRs) are first separated from the fission products and remaining uranium; and then fabricated into fuel that is recycled in advanced reactor systems. The multi strata fuel cycle illustrated in Figure 1 can be changed to accommodate many different fuel cycle options [2] .

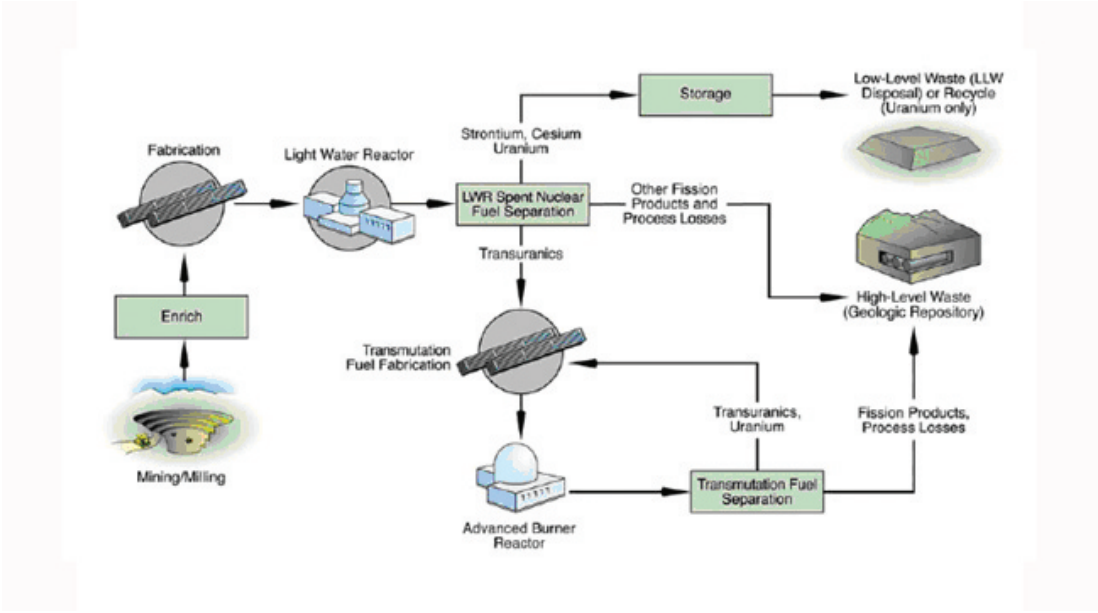

Figure 1: Multi Strata Transmutation Fuel Cycle [2]

This figure illustrates a fuel cycle in which the spent fuel in LWRs is reprocessed and recycled in fast burner reactors. The SNF from the fast reactors is then reprocessed and the fission products and transuranics (TRU) in the waste stream are the only part of the spent fuel to be permanently interned in geological repositories. This method will minimize the number of geological repositories necessary for future storage.

An interesting variant of this method of burning the transuranics is to utilize a subcritical fast burner reactor with a variable strength fusion neutron source. A subcritical system allows for more flexible fuel cycles with the potential to process more transuranics per unit power produced and with fewer reprocessing steps, ultimately leading to fewer burner reactors and fewer repositories being needed.

Such subcritical reactors with a fusion neutron source are known as fusion-fission hybrid (FFH). Subcritical burner reactors with accelerator spallation neutron sources have also been investigated [26]. The fusion neutron source is chosen because the

source strength is variable. It can be raised or lowered readily to maintain a predetermined fission power depending on the changes in reactivity throughout the cycle. Furthermore, the distributed fusion neutron source is better suited for irradiating large reactor fuel volumes than is the more concentrated accelerator neutron source.

There are multiple options when considering the development of a multi-strata fuel cycle. The fuel cycle can incorporate an intermediate recycling step, such as mixed oxide fuel in LWRs, before being recycled in fast reactors for transmutation, or the discharged fuel from LWRs can be directly recycled in a burner/breeder reactor. The burner/breeder reactor system can consist of either conventional fast reactors, or of subcritical fast reactors, or of a combination of the two.

This thesis will focus on examining a fuel cycle for a fusion-fission hybrid reactor that achieves a high burn up limited by radiation damage. Achieving a relatively flat power distribution is also an objective. The limit on the residence time of the fuel in the reactor is the fuel clad lifetime due to radiation damage. Since the reactor employs a 14-MeV neutron source plus a fast fission spectrum the radiation damage per neutron is much higher than in a thermal reactor. Therefore the neutron damage fluence limits for a fast burner reactor are lower than those for a thermal reactor. This study will examine and quantify the type of fuel cycle that can be obtained with a variable strength fusion neutron source that can be available in the next 25-30 years.

CHAPTER II

BACKGROUND

Transmutation of spent nuclear fuel via subcritical systems has been looked at for many years. Subcritical reactors necessitate an external source of neutrons to supplement the neutrons produced via fission in the reactor core. The external source needs to be strong enough to produce enough neutrons to maintain a given fission power level throughout the lifetime of the reactor. The most commonly suggested method of producing an external source of neutrons is through the means of an accelerator. This study utilizes a fusion neutron source based on ITER physics as the neutron source [14].

2.1 Advantages of Subcritical Transmutation

Many transmutation systems have been looked at in the past to reduce the amount of spent fuel that must be stored in a geological repository [30]. These systems include a two-tier system in which only the plutonium from the SNF is recycled in MOX systems and the rest of the minor actinides are placed into a repository along with the fission products. The thermal spectrum of a MOX system is not conducive to burning minor actinides due to the lower fission to capture ratio of minor actinides in a thermal spectrum as compared to a fast spectrum. Fast reactor systems, specifically metal cooled fast reactors, have been investigated for a multi-strata system in which all of the transuranics from LWRs can be recycled. These fast systems have a smaller delayed neutron fraction because of the substitution of Pu^{239} or U^{233} for U^{235}, and less fertile isotopes which have a larger delayed neutron fraction. Furthermore, the effective delayed neutron fraction is smaller due to delayed neutrons being born at lower energies; making them more likely to be parasitically absorbed than prompt

neutrons in a fast spectrum. The smaller effective delayed neutron fraction results in a smaller margin to prompt criticality, a safety issue in case of a reactor transient. A subcritical system can work in a fast spectrum without the worry of the small delayed neutron fraction because there is already a large margin to prompt criticality set in the design phase. Another advantage of the subcritical system is the ability to load the reactor with uranium free fuel. The advantage of a fuel free of U^{238} is that U^{238} will capture neutrons and produce more transuranics during the cycle. In general, transuranics has a higher fission to capture ratio than U^{238} in a fast spectrum. The higher fission to capture ratio results in a greater net rate of transmutation of SNF than in a critical system.

Subcritical systems can achieve a deeper burnup than their critical counterpart. Critical systems are limited in that criticality must be maintained to sustain the fission reaction. But a subcritical system is limited by the strength of the external source of neutrons not criticality concerns. The stronger the neutron source strength the greater the potential burnup that can be achieved in the system. The limiting concerns for a subcritical system are the radiation damage to materials in the core, specifically the cladding of the fuel, and radial power peaking factors; which if too high cause a problem in effectively cooling the core during a transient.

2.2 Advantages of Fusion-Fission Hybrid Reactors

Fusion-Fission hybrid reactors have an advantage over accelerators for neutron production in that the neutron source strength is variable in a FFH as opposed to accelerators. An accelerator is designed to operate at a specific current and voltage level provinding a fixed number of neutrons. Operating the system at a smaller current and voltage is possible but not economical. The ability to operate at a lower power level than the design limit allows for a change in reactivity throughout the fuel cycle while maintaining the same thermal power level. The required fusion power, P_{fus}, for

a given reactivity is determined by the fission power level, P_{fis}, the neutron multiplication of the source, k, the neutrons released per fission event, ν, the energy released per fusion event, E_{fus}, and the energy released per fission event, E_{fis}.

$$P_{fus} = P_{fis} \times \frac{1-k}{k} \times \nu \times \frac{E_{fus}}{E_{fis}} \tag{1}$$

The fusion power level is adjusted by either increasing the external heating of the plasma or by increasing the fuel density. Increasing the external heating of the plasma is accompolished via lower hybrid heating or neutral beam injection.

2.3 Evolution of Subcritical Advanced Burner Reactor (SABR)

The fusion fission transmutation concept has been studied for many years at the Georgia Institute of Technology. The design started with the Fusion Transmutation of Waste Reactor (FTWR) [34]. The FTWR is a lead lithium cooled subcritical reactor that was capable of reducing the transuranic content of SNF by 99%.

The next iteration in the Georgia Tech FFH design was the Gas Cooled Fast Transmutation Reactor, GCFTR, which attempted to reduce the transuranic content of SNF without reprocessing [35, 36]. The GCFTR was a gas cooled subcritical fast fission fusion hybrid, fueled with a TRISO fuel particle in an effort to achieve a deep burn of transuranics in a once through cycle. The achieved burnup in the GCFTR was maximized at 94% burnup [38].

2.3.1 SABR Design

SABR is a fusion fission hybrid reactor combining ITER physics and technology and combining it with the leading sodium cooled fast reactor technology. Figure 2 is a simplified three dimensional model of the reactor. The fusion plasma shown in yellow is surrounded on the top and bottom by a lithium orthosilicate (Li_4SiO_4) tritium breeding blanket and on its outboard side by a subcritical transuranic fission core (in

red). The fission core has been designed to accommodate three different fuel types, two metallic fuels and one oxide fuel: a TRU-Zr metal fuel and a TRU-MgO metallic fuel, as well as a TRU-MgO oxide fuel. The subcritical fission core is also surrounded on the top and its outside by a Li_4SiO_4 blanket. After the tritium breeding blankets there is a stainless steel neutron reflector used to return neutrons back into the system either to be captured in the tritium breeding blanket or possibly to be transmuted in the subcritical core. Outside of the stainless steel reflector is a multi-layered shield to capture neutrons and gamma rays and protect the toroidal field magnets.

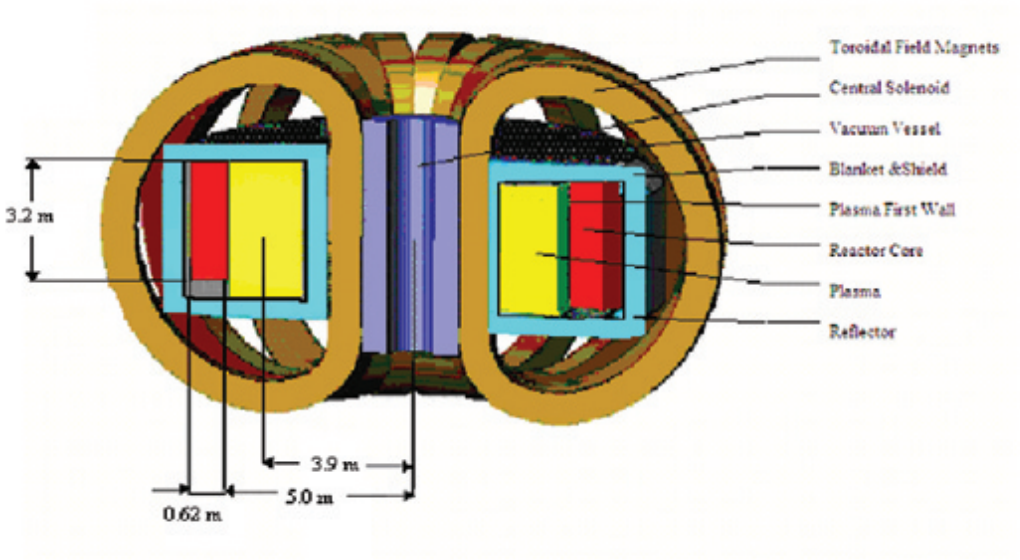

Figure 2: Three Dimensional Schematic for SABR

The fission core is 3.2 meters in height; the active fuel region is 2.0 meters in height with a 1.0 meter plenum for fission gases and a 20 cm stainless steel reflector on top of the fission gas plenum. The fuel is arranged in hexagonal assemblies, with each fuel assembly having either 271 pins per assembly or 169 pins per assembly depending on the fuel that is being burned in the reactor.

2.3.1.1 Fuel Element and Fuel Assembly Design

The fuel SABR was designed for is the TRU-Zr metal fuel from Argonne National Laboratory (ANL) [29]. The fuel is composed of 40Zr-40Pu-10Np-10Am by weight percent. The isotopic composition of the fuel is given in Table 1. The metallic fuel form was chosen because it has a high thermal conductivity, high fission gas retention, and the ability to contain a high density of actinides. The high fission gas retention allows for the fuel to be irradiated to greater burnups.

Table 1: ANL Fuel BOL TRU Composition [29]

	Mass Percent
Isotope	Beginning of life (BOL)
Np^{237}	17.0
Pu^{238}	1.4
Pu^{239}	38.8
Pu^{240}	17.3
Pu^{241}	6.5
Pu^{242}	2.6
Am^{241}	13.6
Am^{243}	2.8

The geometry of SABR's fuel pin differs from that of a traditional metallic fuel pin in that it is composed of four different components instead of three, as in a traditional metallic fuel pin. The fuel slug is bonded to the cladding by a sodium gap. The sodium bond provides good thermal conduction between the fuel and the clad until the fuel swells into contact with the clad during irradiation and the sodium bond is displaced. The cladding is oxide dispersion strengthened (ODS) steel, which is currently under development and is supposed to be able to withstand higher irradiation damage rates

than the current steel used as cladding in fast reactors today. Outside of the cladding is a thin layer of lithium niobate ($LiNbO_3$). The lithium niobate is used as an electrical insulator. This insulator is necessary because SABR is cooled by pumping a liquid metal through a magnetic field. The $LiNbO_3$, acting as an insulator, breaks up the magnetic field in the fission core, which would inhibit coolant flow in the core via a large magneto-hydrodynamic pressure drop. Figures 3 and 4 below are radial and axial images of SABR's fuel pins.

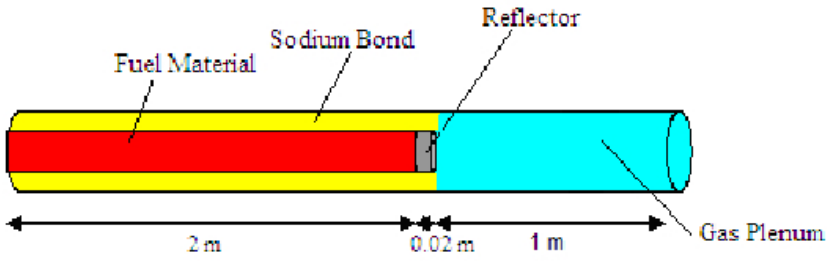

Figure 3: Axial View of SABR Fuel Pin

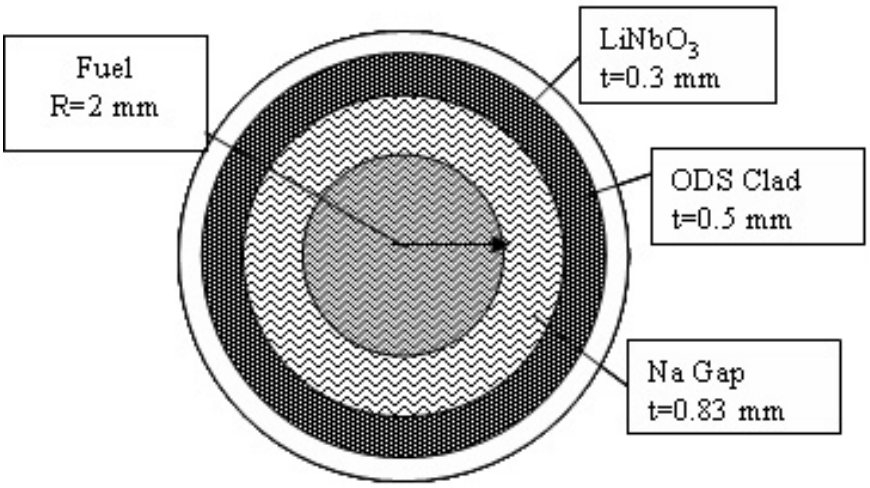

Figure 4: Cross-Section of Metallic ANL-Fuel Pin

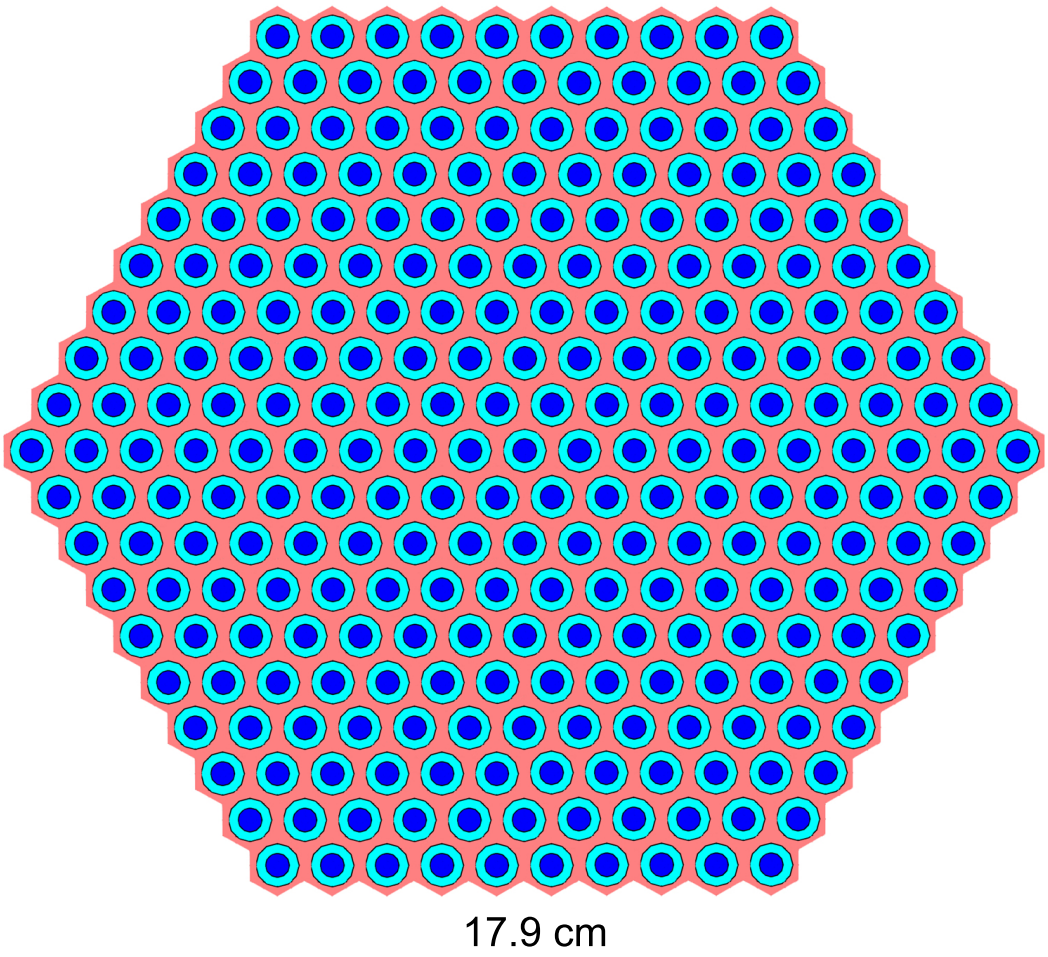

Figure 5: Cross-Section of SABR Metallic Fuel Assembly

2.3.1.2 SABR Minor Actinide Burning Fuel

In this study SABR, also operates with a Minor Actinide (MA) burning fuel [5]. The MA-Oxide fuel was designed for use in EFIT, European Facility for Industrial Transmutation [6]. EFIT is a 400 MW_{th} subcritical reactor driven with the external source of neutrons provided by an accelerator. EFIT was designed with the primary purpose of burning minor actinides from SNF without a high transmutation rate of plutonium. The European fuel cycle strategy is to save the plutonium discharged from LWRs for future fast reactor systems and to destroy all remaining minor actinides in

EFIT type systems. The EFIT design requires a change in reactivity over time that is quite small since accelerators are a fixed external neutron source strength. The fuel is composed of transuranics embedded in a magnesium oxide matrix (MgO) in the proportions of 60% transuranics and 40% MgO by volume. The transuranics is comprised of 54.3% minor actinides and 45.7% plutonium by weight, the plutonium and minor actinide fuel vectors are listed in Table 2.

Table 2: Minor Actinide Burning Fuel Vector for the Minor Actinide Burning Fuel [12]

Plutonium Vector		Minor Actinide Vector	
Isotope	Mass Percent	Isotope	Mass Percent
Pu^{238}	3.73	Np^{237}	3.884
Pu^{239}	46.446	Np^{239}	0.0
Pu^{240}	34.121	Am^{241}	75.51
Pu^{241}	3.845	Am^{242m}	0.254
Pu^{242}	11.850	Am^{242f}	0.000003
Pu^{243}	0.0	Am^{243}	16.054
Pu^{244}	0.001	Cm^{242}	0.0
		Cm^{243}	0.066
		Cm^{244}	3.001
		Cm^{245}	1.139
		Cm^{246}	0.089
		Cm^{247}	0.002
		Cm^{248}	0.0001

The oxide fuel, having a lower heavy metal density than metallic fuel, needs to compose a larger volume of the fuel area in order to achieve a high enough reactivity to

be supported by the fusion neutron source. This results in the oxide fuel pin having a larger pin diameter and a smaller coolant to fuel volume ratio. This is possible because the oxide fuel has a much greater melting temperature than the metallic fuel, approximately 3,000 k for oxide fuels and 1,350 k for metallic fuels [31]. This results in a new fuel assembly that has the same outer dimensions of the metallic fuel assembly but contains 217 fuel pins instead of 271. Each fuel pin will now have an outer fuel diameter of 8.72 mm as compared to 7.36 for the metallic fuel. Figures 6 and 7 are a representation of the redesigned fuel pins and fuel assemblies for the oxide fuel.

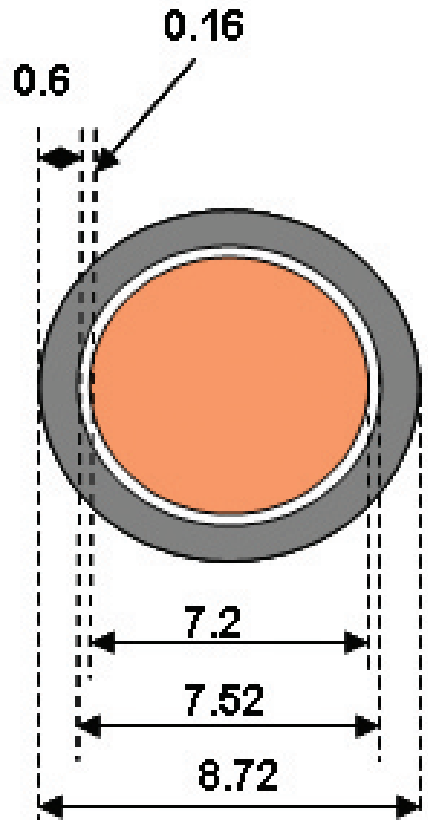

Figure 6: Cross-Section of SABR MA-Oxide Fuel Pin

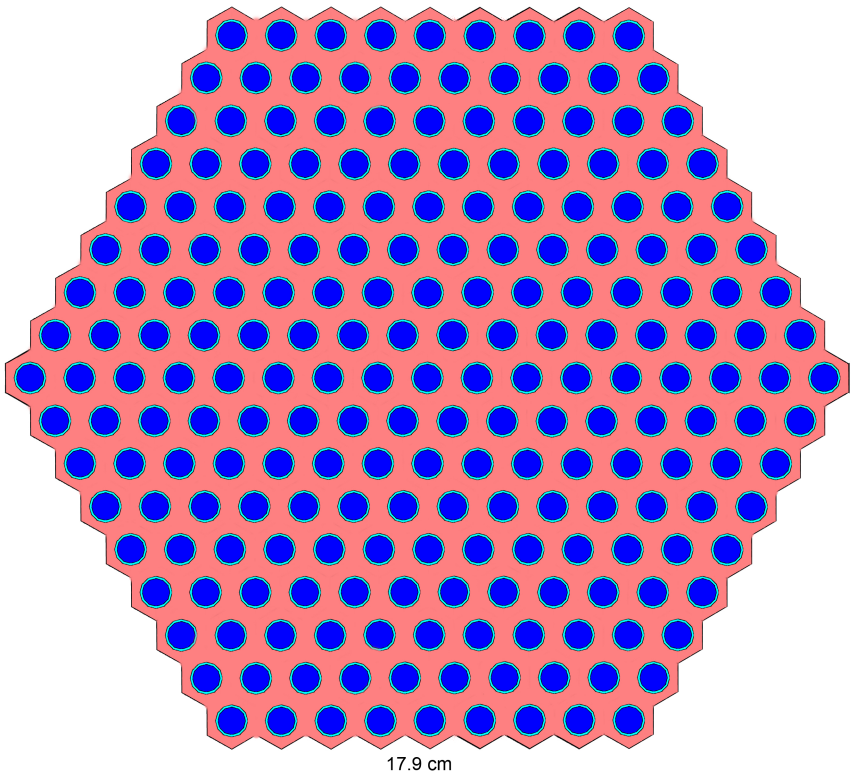

Figure 7: Cross-Section of SABR MA-Oxide Fuel Assembly

Table 3 is a comparision of the major parameters for the oxide and metal fuel pins and fuel assemblies [38].

2.3.1.3 Tritium Breeding Blanket

A design goal of SABR is for the reactor to be tritium self sufficient. To achieve this goal it is necessary to surround both the fusion plasma and the fission core with a tritium breeding blanket. The tritium blanket in SABR is composed of lithium orthosilicate (Li_4SiO_4) with channels for both tritium collection and sodium coolant. Lithium orthosilicate was chosen for the breeding blanket material because the material has a high lithium density as well as a low probability of forming hydroxides [37]. The reactor is composed of two breeding blankets; one blanket that surrounds the fusion plasma and one surrounding the fission core. The blankets are composed

Table 3: Key Design Parameters for the SABR Metal and Oxide Fuel Pin and Assembly

Parameter	Metal	Oxide	Parameter	Metal	Oxide
Rod Length (m)	3.2	3.2	$\frac{Volume_{Plenum}}{Volume_{fm}}$	1	0.8
Length of Fuel Material (m)	2.0	2.0	Total Pins in Core	248778	155142
Length of Plenum (m)	1	1	Diameter Flat to Flat (cm)	15.5	15.5
Length of Reflector (m)	0.2	0.2	Diameter Point to Point (cm)	17.9	17.9
Radius of Fuel Material (mm)	2.0	3.6	Length of Side (cm)	8.95	8.95
Thickness of CLad (mm)	0.5	0.3	Pitch (mm)	9.41	13.63
Thickness of Na Gap (mm)	0.83	0.16	Pitch to Diameter Ratio	1.3	1.56
Thickness of Lithium Niobate (mm)	0.3	0.3	Total Assemblies	918	918
Rod Radius with Clad (mm)	3.63	4.36	Pins per Assembly	271	169
			Coolant Flow Area per Assy (cm^2)	96	108

of lithium orthosilicate but differ in the isotopic content of lithium in the blanket. Natural lithium is composed of Li^6 and Li^7 at concentrations of 7% and 93% respectively. The two different breeding blanket compositions are used to take advantage of a softer neutron spectrum coming out of the fission core as opposed to the fusion plasma. The absorption cross sections of Li^6 and Li^7 are quite similar at these high energies; while the neutrons that leave the fission core will be at much lower energies, where the absorption cross section of Li^6 is much higher than Li^7, as shown in Figure 8.

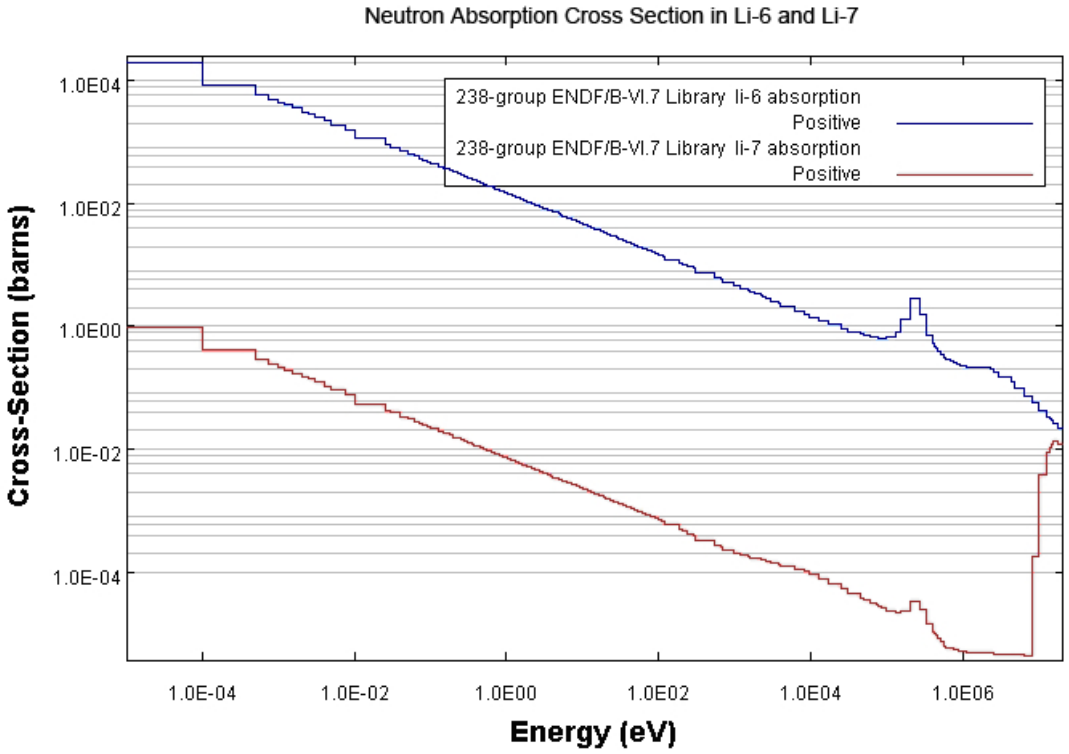

Figure 8: Lithium (n, α) Cross Section Comparison

The tritium generated throughout the cycle is removed continuously using a helium purge gas. The reason for the continuous removal of tritium is with a relatively short half life (≈12 years) and a cycle length of 2 years a significant portion of tritium would decay throughout the cycle.

Typical fast reactors have peak neutron energies between 100 KeV and 1 MeV, where the Li^6 absorption cross section is 3-4 orders of magnitude higher than that of Li^7. Equation 2 is the relationship between tritium production in the system, the neutron flux, the amount of lithium in the system, and the (n, α) cross section in lithium.

$$P_T = \sum_{Li^6, Li^7} \int \int \phi(r, E)\sigma(n, \alpha)(E)N_{Li}dEdV \tag{2}$$

P_T is the tritium production at a given time, $\sigma(n, \alpha)$ is the microscopic (n, α) cross section, and N_{Li} is the number density of lithium. The destruction rate of tritium is directly proportional to the fusion power and the energy released per fusion event.

$$D_T = \frac{P_{fusion}}{E_{fusion} \times Q} \tag{3}$$

In equation 3 D_T is the destruction rate of tritium, P_{fusion} is the fusion power, E_{fusion} is the amount of energy released per tritium atom fused in MeV, and Q is the elementary charge. The neutron flux in the system is dependent on the fusion power and the multiplication of the source.

$$\phi(r, E) = f(P_{fusion}, k) \tag{4}$$

This shows that the tritium production and destruction rate are coupled to each other through both the fusion power and the resulting neutron flux. The tritium production and destruction are necessary to calculate the net gain of tritium at any point in time in the system. The instantaneous rate of change in tritium atoms is calculated by

$$\frac{dN_T}{dt} = P_T(t) - D_T(t) - \lambda N_T(t) \tag{5}$$

where N_T is the number density of tritium in the system and λ is the decay constant of tritium. The amount of tritium breeding is calculated by integrating this equation over time resulting in the net tritium gain in the system at any point in time.

2.3.1.4 Fusion Neutron Source

Conservative ITER-like physics was adopted for the design of the SABR tokamak neutron source. Fusion powers, between 100 and 500 MW_{th} are required to support 3000 MW_{th} of fission power in the range of subcritical operation envisioned. A reference normalized ratio of plasma-to-magnetic pressure β_N of 2.0-2.5% was chosen, although operation at β_N values up to 3.0% could be justified on the basis of present experience. An energy confinement multiplier H of 1.0-1.1 relative to the presently achieved IPB98(γ,2) energy confinement scaling was adopted. The line average electron density was fixed at 75% of the empirical Greenwald density limit to avoid confinement degradation at higher densities. An edge safety factor q_{95} of 3 was specified to avoid MHD kink instabilities. For a R = 3.75 m tokamak a range of operating parameters are possible [10]. The ITER single null divertor (not shown in Figure 10) and first wall were adapted for sodium coolant by scaling down to the SABR dimensions with the same coolant channels.

The heat removal capability was confirmed by detailed FLUENT code calculations. The ITER Lower Hybrid (LH) heating and current drive system was adapted to provide 100 MW of heating and to drive 7.5 MA of plasma current. The superconducting magnet systems for SABR were directly adapted [14] from the ITER cable-in-conduit Nb_3Sn conductor surrounded by an Incoloy 908 jacket and cooled by a central channel carrying super-cooled helium, with maximum fields of 11.8 and 13.5 T, respectively. The dimensions of the central solenoid coil were constrained by the requirement to provide inductive startup and to not exceed a maximum stress of 430 MPa set by matching ITER standards and Incoloy properties. The dimensions of the 16 toroidal field coils were set by conserving tensile stress calculated as for ITER, taking advantage of an Incoloy 908 jacket for support. The major parameters of the SABR design are summarized in Tables 4 [38] and 5 [10].

Table 4: Major Parameters for the Fission Core in SABR [38]

Fission Core	
Fission Power	3000 MW_{th}
TRU Fuel Composition (weight percent)	Pu-40, Am-10, Np-10, Zr-40
Fuel Density	9.595 g/cc
Mass of TRU Mass of Fuel Material	32 MT 53 MT
Specific Power	93.75 kw_{th}/kg TRU
Maximum k_{eff}	0.95
Major Dimensions	R_{in} = 5 m, R_{out} = 5.62 m H_{active} = 2 m
Coolant mass flow rate Temperature	$\dot{m}$ = 8700 kg/s T_{in}, T_{out} = 377, 650° C
Power Density	$q''' = 72.5$ MW/m^3
Linear Fuel Pin Power	6 kW/m
Clad, Wire Wrap, and Flow Tube	ODS Ferritic steel t = 0.5 mm, 2.2 mm, and 2.0 mm
Reflector, Blanket, and Shield	
Reflector and Shield Materials	ODS Steel, Boron Carbide Tungsten, Na Cooled
Tritium Breeder	Li_4SiO_4
Combined Thickness	80 cm
Coolant mass flow rate	$\dot{m}$ = 0.2 kg/s
Min and Max Blanket Temperatures	T_{min} = 450° C , T_{max} = 640° C

Table 5: Major Parameters for the Fusion Neutron Source in SABR [35]

Plasma	
Plasma Current	8-10.0 MA
Fusion Power Neutron Source Rate	50-500 MW 1.8e19 s^{-1} to 1.8e20 s^{-1}
Fusion Gain	3.2
Superconducting Magnets	
Field Central Solenoid Torodial Field Coil Plasma Center	13.5 T 11.8 T 5.9 T
Torodial Field Coil Dimensions	width = 5.4 m height = 8.4 m $\text{thickness}_{radial}$ = 43 cm $\text{thickness}_{torodial}$ = 36 cm
Divertor	
Materials	Tungsten, CuCrZr, Na cooled
Heat Flux	1-8 MW/m^2
Coolant Mass Flow Rate	$\dot{m}$ = 0.09 kg/s
First Wall	
Materials	Beryllium on ODS, Na Cooled
Surface Area	223 m^2
Average Neutron Wall Load (14 MeV)	1.0 MW/m^2
Average Heat Flux (500 MW)	0.25 m^2
Coolant Mass Flow Rate	$\dot{m}$ = 0.057 kg/s

2.4 Reprocessing

Reprocessing of nuclear fuel has many political hurdles as well as technological hurdles. A closed fuel cycle as envisioned in SABR necessitates reprocessing of spent fuel. One method of reducing the proliferation risk of these fuel cycles is to have an international fuel bank where only a few countries have have the ability to reprocess and the countries without reprocessing capablities are guaranteeed fuel at fair market value. The countries that will have the ability to reprocess will do so under international oversight and control [19]. Also to further reduce the proliferation risk in fast reactor systems it is possible to recyle the plutonium together with the actinides and some fission products (so that it never appears in a fuel form sutiable for nuclear weapons without substantial processing) [16].

The two reprocessing methods currently being researched in the United States are the UREX+ process [22] and Electrochemical reprocessing. The UREX+ process is a form of aqueous reprocessing that does not separate the plutonium from the rest of the transuranics as it is done in the PUREX process. Electrochemical reprocessing methods use oxidation reduction reactions in order to separate the transuranics and the fission products from the uranium in a non-aqueous media.

2.4.1 Aqueous Reprocessing

The UREX process was born out of PUREX technology. The UREX process is necessary due to several issues in the PUREX process that include minor actinides being sent to the waste repository; which increases radiotoxicity, long term heat generation, and volume of waste. Furthermore, the PUREX process separates out a pure plutonium stream and use in a civil setting violates the national policy of the United States.

The UREX process corrects both of these issues. First, the plutonium is never separated out in a pure stream. The plutonium is either separated out with all of

the transuranics or in a stream with neptunium. The UREX process also separates out the long lived fission products (Tc, I) and the short term high heat producing fission products (Cs, Sr). The separation of the long lived fission products is for dose management and the separation of the short term is for heat management issues at emplacement of the fuel [15]. The UREX process also separates the minor actinides out for short term storage and recycle in fast reactor systems. Table 6 shows the recovery efficiency of key elements in the UREX+1a process.

Table 6: Recovery Efficiency of Key Elements in UREX Process [15]

Element	Recovery Efficiency
Uranium	99.9992%
Technetium	98.3%
Cesium	>99.2%
Strontium	>99.9%
Plutonium	>99.99%
Neptunium	>99.99%
Americium	>99.99%
Curium	>99.999%

2.4.2 Electrochemical Reprocessing

Electrochemical reprocessing methods use oxidation reduction reactions in order to separate the transuranics and the fission products from the uranium in a non aqueous media. This method utilizes differences in volatility and thermodynamic stabilities of the elements to achieve separation [12]. The electrochemical processes were developed for the fast reactor fuel cycle. This means of reprocessing was pursued for multiple reasons. First, the facility is more compact and can be co-located at a reactor site. Co-locating the reprocessing facility at the reactor site reduces transportation risks

and accomodates more precise monitoring of plutonium. Second, Fast reactor fuel does not require a high degree of decontamination. The lower degrees of decontamination allow for all of the transuranics to be separated out in one step and never solely separating out the plutonium. Third, resistance to radiation effects allows the fuel to be reprocessed with a shorter cooling time. Fourth, it is compatible with advanced fuel types. Lastly, it is capable of low purity products [12]. The ability to co-locate the reprocessing facility, more precisely monitor the plutonium, separating out all of the TRU and not solely the plutonium, and having a higher dose rate fuel from not having to cool the fuel as long before reprocessing are non-proliferation advantages to electrochemical reprocessing over an aqueous system. This investigation simulates electrochemical reprocessing under development at Argonne National Laboratory [7] because of the metallic fuel choice. The choice of electrochemical reprocessing eliminates the additional oxidation step that is necessary to convert the fuel into a form compatible with aqueous reprocessing methods.

CHAPTER III

SABR FUEL CYCLE

The purpose of this study is to determine the potential benefits of several transmutation fuel cycles on closing of the nuclear fuel cycle through the simulation of several fuel cycle strategies. The strategies to be examined include: the length of the fuel cycle versus accumulated radiation damage, rotation of the fuel assemblies throughout the cycle, and fuel composition. For a proper comparison to be made the baseline power level in each case needs to remain constant. The fuel cycles will be compared against the current method of fuel disposal in the United States of a once through cycle on the basis of decay heat produced. The fuel cycles will also be compared against the EFIT system and a representative fast reactor.

3.1 SABR Fuel Cycle

The reactor system utilized in this study is the SABR system. SABR utilizes the out-to-in shuffling pattern found in Figure 9 below.

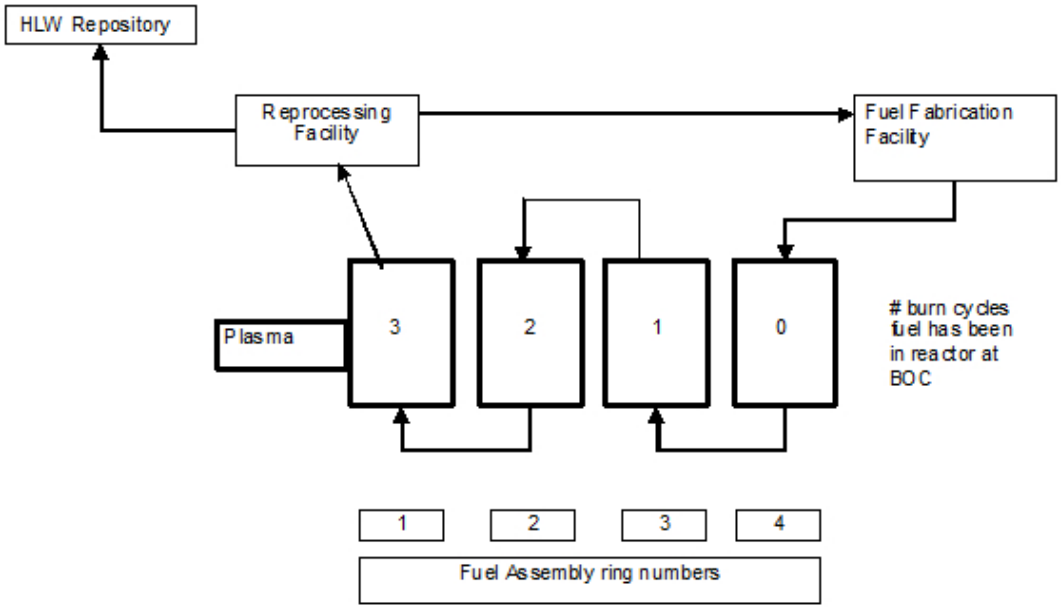

Figure 9: In to Out Shuffling Pattern for the SABR Fuel Cycle

At beginning of life (BOL) fresh fuel is placed in all four regions of the core. When the fuel has been irradiated for its cycle time, each fuel assembly is shuffled one ring inward; with the innermost ring (ring 1 in the diagram) being removed from the core and sent to the reprocessing facility. This is where the fission products are removed from the transuranics and sent to the repository and the remaining transuranics is sent back to the fuel fabrication facility, where it is combined with fresh transuranics from light water reactors. It is here where new fuel elements and assemblies are manufactured and then placed back into the reactor.

CHAPTER IV

COMPUTATIONAL TOOLS

To perform the required simulations necessary for the study, two primary software packages were used: ERANOS2.0 [24] and ORIGEN-S [21]. The ERANOS2.0 package includes the ECCO cell and lattice code, deterministic flux solvers, burn up module, and multiple post processing options. This investigation uses ERANOS2.0 to calculate the full core flux distribution, the power distribution, full core burn up, and radiation damage to the components. ORIGEN-S was used to calculate the decay heat of the discharge fuel from SABR. ERANOS2.0 does not track the necessary number of nuclides for decay calculations so the discharge compositon is translated into ORIGEN-S for the decay calculations.

4.1 ERANOS2.0

The European Reactor Analysis Optimized calculation System, ERANOS, was developed and validated at CEA for neutronic calculations of fast reactor systems. The code has many modules that can either be used in a stand-alone form or linked together to model and analyze the behavior of nuclear reactors.

The cross-section libraries in ERANOS2.0 are generated from JEF-2.2 cross sections. The cross sections were processed via the NJOY [17] and CALENDF [40] software codes to generate the appropriate subgroup parameters that reflect the resonance cross-sections. ERANOS then uses a cell and lattice code, ECCO, to generate problem specific libraries. Fast reactor lattice cells have special characteristics for which special treatments are provided in ECCO: elastic slowing down of neutrons by light and intermediate elements, discrete treatment of the inelastic reaction, self-shielding effects in the 100 keV-1 keV range are treated, by the narrow resonance

approximation, and treatment of streaming effects, which are important in sodium voided cells.

Utilizing a 2-D model of a fuel assembly in the reactor, ECCO uses a variety of slowing down treatment methods over multiple groups. The subgroup method is used within each group to generate the cross-sections. ECCO contains 1968 groups for the most important nuclides in the reactor (fuel and coolant materials), and uses either 33 or 172 groups for the less important nuclides (structural materials). The following is the formulation used to calculate a generic cross section σ_x in ECCO

$$\tilde{\sigma}^g_{xi} = \frac{\sum_j S^g_j \sum_k \alpha^g_k \sigma^g_{x_k} P_{ij}\left(\Sigma^g_{t_k}\right)}{\sum_j S^g_j \sum_k \alpha^g_k P_{ij}\left(\Sigma^g_{t_k}\right)} \tag{6}$$

S^g_j is the source term in group g of region j, k_g is the probability of each partial cross-section in group g, and $Pij\Sigma(tkg)$ is the reduced collision probability between regions I and j for subgroup k within group g [23]. Equation 7 is the formulation of total cross section of Legendre order one, which requires current weighting.

$$\tilde{\sigma}_{t_{li}} = \frac{\sum_j S_j \sum_k \alpha_k \sigma_{t_{lk}} \sum_l P_{il}\left(\Sigma_{t_k}\right) P_{lj}\left(\Sigma_{t_k}\right)}{\sum_j S_j \sum_k \alpha_k \sum_l P_{il}\left(\Sigma_{t_k}\right) P_{lj}\left(\Sigma_{t_k}\right)} \tag{7}$$

The flux and current for the system are calculated from the self-shielded cross-sections generated in ECCO. The cross-sections in the group structure prescribed for the problem is produced by collapsing the self-shielded cross-sections and smearing them over the subassembly.

To perform the core calculations in this study, ERANOS uses a discrete ordinates transport code called BISTRO [11]. This study uses a S-8 quadrature set to discretize the angular flux and diamond differencing for the spatial discretization. The BISTRO calculation generates the flux and power profiles that are used for the burn up calculation, in the EVOLUTION [8] module. EVOLUTION takes as an input the

reactor geometry and the average flux profile in the system, as well as a time period to burn the fuel. The fuel irradiation time is broken up into multiple time steps to account for changes in the flux profile over time. The flux profile from BISTRO is then used to calculate the radiation damage to the cladding. The flux is called into a post processing module which calculates the maximum radiation damage at a specific time. This can be done for multiple steps to obtain the damage rate at certain points in time and then interpolated between time steps to obtain the cumulative radiation damage to the cladding.

4.2 ORIGEN-S

ORIGEN-S is an irradiation and decay code developed by Oak Ridge National Lab. In this paper the code will be used to decay the transuranics and fission products that result from the simulation of the fast reactor fuel cycles in ERANOS. ORIGEN-S is capable of decaying the fuel for thousands of years in multiple time steps where as ERANOS is only capable of one decay step. ORIGEN-S utilizes the Bateman equation to track the buildup and decay of isotopes over time.

$$\frac{dN_A}{dt} = -\lambda_A N_A - \left[\sum_g \sigma_{ag}^A \phi_g\right] N_A + \lambda_B N_B + \left[\sum_g \sigma_{\lambda g}^C \phi_g\right] N_C \tag{8}$$

where $\lambda_A N_A$ is the loss due to radioactive decay of A, $\left[\sum_g \sigma_{ag}^A \phi_g\right] N_A$ is the loss due to neutron capture by A, $\lambda_B N_B$ is the gain due to decay of B to A, and $\left[\sum_g \sigma_{\lambda g}^C \phi_g\right] N_C$ is the gain of due to transmutation of C to A via neutron capture [9].

The use of ORIGEN-S ensures that all possible decay branches are considered throughout the 1 million years of radioactive decay that will be simulated. The output of ORIGEN-S will be the decay heat contributions of both the transuranics and the fission products. This will allow for a comparison of just the transuranics from each of the fuel cycles as well as the transuranics from a light water reactor.

4.3 Computational Model

SABR was modeled in a multi tiered approach in ERANOS2.0. First the fuel and tritium blanket assemblies were modeled heterogeneously in complete detail. The shield, plasma and superconducting magents were modeled as homogenous medium. The cross sections were processed on these assemblies and homogenized to conserve reaction rates. Figure 10 illustrates the computational model used in ERANOS.

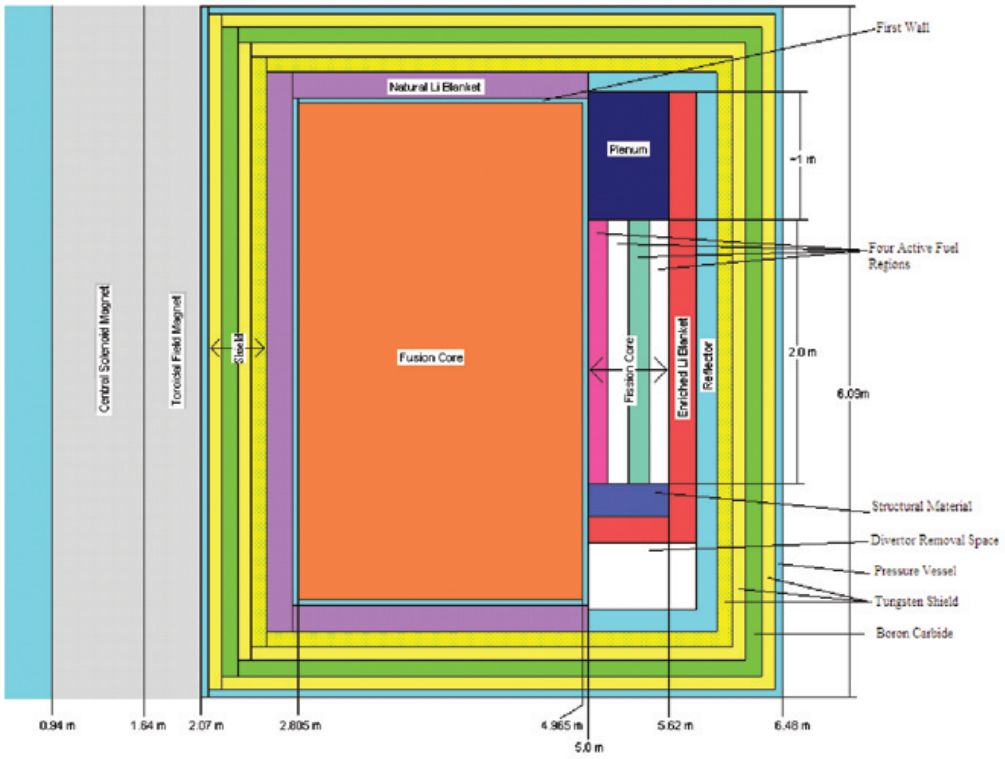

Figure 10: SABR RZ Computational Model used in ERANOS2.0

The torodial plasma has been converted into a cylinder in RZ coordinates and the volume of the plasma region is conserved. Converting the plasma from a torus to a cylinder is acceptable because the volume of the region as well as the overall strength of the fusion source is conserved. The fusion source is modeled in ERANOS as a volumetric source with a neutron energy in the energy group between 12 MeV

and 17 MeV, this results in a slight difference in neutron energy from the 14.1 MeV neutrons produced in a fusion reaction. The slightly higher average neutron energy in the computational model (14.5 MeV) results in higher radiation damage to the structural materials in the reactor.

The radii of each of the assembly rings in the core preserve the volume of the hexagonal fuel that makes up each ring of assemblies. Each ring of fuel assemblies in the fission core is divided into 2 rings, an inner ring and an outer ring, to facilitate the rotation of the fuel assemblies throughout the fuel cycle. The model has 92 radial mesh points and 94 axial mesh points, of which 24 radial and 20 axial mesh points are in the fission region.

The neutron flux and subsequent depletion calculations were simulated every 250 days, this is because the depletion module in ERANOS uses an average flux at a specific time step for the depletion calculations. The change in both the magnitude of the flux profile and the flux spectrum over these 250 day intervals is minimal and yields a valid assumption of the average neutron flux over all 250 days.

CHAPTER V

FUEL CYCLE SIMULATIONS

A series of fuel cycle simulations were evaluated for the SABR transmutation system to determine which set of parameters resulted in the most desirable fuel cycle. The fuel cycles simulated were limited by accumulated radiation damage versus burnup, transuranic fuel vector, metallic or oxide fuel choice, and rotation of the fuel assemblies.

Each fuel cycle simulation was evaluated based on multiple performance indicators: burnup, total transuranic destruction, total plutonium destruction, total minor actinide destruction, required fusion power, power peaking, light water reactor support ratio, radiation damage, decay heat to the repository, and tritium breeding.

The fuel burnup is proportional to the power level, the fuel residence time in the reactor, and the initial amount of transuranics in the system at beginning of cycle (BOC). The fuel burnup in SABR is defined by the amount of Fissions per Initial Heavy Metal Atom (FIMA).

$$FIMA = \frac{Initial - Final}{Initial} \tag{9}$$

Where *Initial* is the the initial amount of transuranics loaded at the beginning of cycle and *Final* is the amount of transuranics that are removed from the reactor at end of cycle. Total transuranic destruction can be broken down into destruction of plutonium and of minor actinides. The fission power level in the reactor and the fuel residence time determine the total transuranic destruction in the system. The ratio of plutonium to minor actinide destruction is dependent on initial fuel vector and flux spectrum in the system. Figure 11 illiustrates that the harder the flux spectrum, the more competitive the fission cross sections of minor actinides come to the fission

cross section of plutonium and thus in a harder spectrum there is a higher ratio of minor actinide destruction than in a softer spectrum.

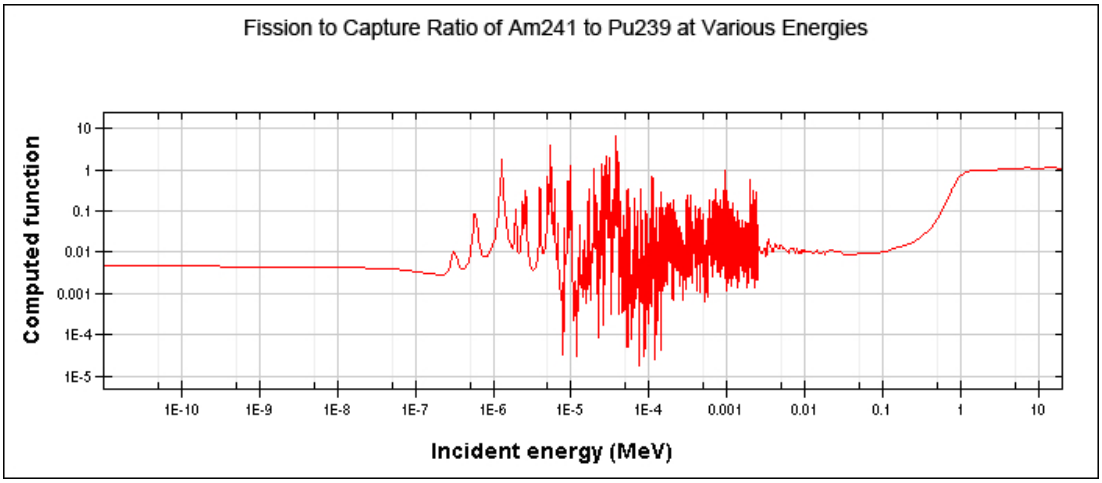

Figure 11: Ratio of Am^{241} Fission Cross Section to Pu^{239} Fission Cross Section

The LWR support ratio is a key figure of merit in this study because it quantifies the ratio between the number of 1000 MW_e LWRs that can be supported by one SABR system. The support ratio is defined as the amount of transuranics destroyed per full power year in SABR divided by the amount of transuranics generated per full power year in a light water reactor. The ratio is dependent on the fission power level of SABR.

The decay heat to the repository is the limiting factor into how much transuranic waste can be stored in a Yucca Mountain type repository. Geological repositories are limited by two different temperature readings, the drift wall temperatures and the mid drift temperature. The drift wall temperature limits are both for emplacement of the fuel and closure of the repository. These limits are near term limits and the decay heat from the fission products is the primarty contributor. The mid drift temperature limit is a long term temperature limit and is mainly affected by the transuranics. Destroying the transuranics in SABR will lower the amount of transuranics in the repository and increase the effective repository space. Figure 12

[32] shows the increase of effective space of a geological repository against separation and transmutation of key isotopes.

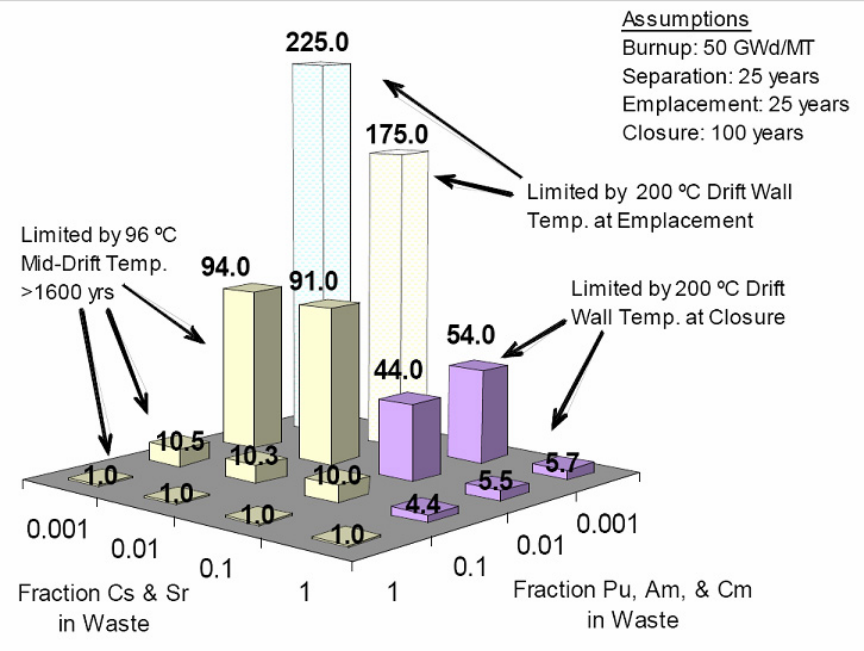

Figure 12: Transmutation and Separation Methods to Increase the Effective Space of Yucca Mountain [32]

Fuel cycles that reduce the long term temperature limits and mid drift temperatures via transmutation of the transuranics produced in LWRs are preferred. Separating out the cesium and strontium to reduce the short term temperature limits was not considered in this study.

Tritium production is necessary in SABR to fuel the D-T fusion neutron source. Tritium is produced in the breeding blankets throughout the cycle. Enough tritium must be produced in the blankets accounting for decay of the tritium (12.2 year half life) for the fusion neutron source to operate. In principle, a tritium breeding ratio (TBR) of 1.0 is sufficient. However, taking into account tritium decay and loss, a TBR of 1.1 is a practical design objective.

5.1 Accumulated Radiation Damage versus Burnup

The first fuel cycle scenario analyzed was the effect of increasing radiation damage on burnup. Simulations were run for SABR's out-to-in shuffling pattern for irradiation times corresponding to 100, 200, and 300 displamcements per atom (dpa), as well as a once through fuel cycle that obtains greater than 90% burnup. These limits were chosen because currently there is no generally accepted upper limit in place on radiation damage in fast reactors. Fast reactors are predicted to operate in the range of 150 to 200 dpa. The 300 dpa limit was investigated to determine if there is a benefit to conducting research into developing new cladding materials able to withstand higher radiation damage. The once through cycle was chosen to see what the necessary radiation damage and fusion power requirements would be as well as the benefits of not having to go through a reprocessing step.

The simulations were run and show that the relationship between radiation damage and burnup is linear in the regime from 100 to 300 dpa. This linear relationship results in linear increases in fusion power and transuranics burned per residence in this regime. The results are summarized in Table 7.

Table 7: Accumulated Radiation Damage versus Burnup Fuel Cycle Results

Parameter				
Cycle	100 dpa	200 dpa	300 dpa	Once Through
Cycle Length (days)	350	700	1000	4550
4 Batch Residence Time (years)	3.83	7.67	10.95	49.8
Fission Power (MW_{th})	3000	3000	3000	3000
FIMA (%)	16.7	23.8	31.6	87.2
Regional Power Peaking				
BOC	1.68	1.80	1.82	1.97
EOC	1.78	1.98	2.04	2.04
BOL P_{fus} (MW)	72	72	72	72
BOC P_{fus} (MW)	155	240	286	1012
EOC P_{fus} (MW)	218	370	461	1602
BOL k_{eff}	0.972	0.972	0.972	0.972
BOC k_{eff}	0.940	0.894	0.887	0.784
EOC k_{eff}	0.916	0.868	0.834	0.581
TRU Burned/yr (kg)	1064	1058	909	545
Support Ratio (100%)	3.86	4.26	4.84	2.90
Support Ratio (75%)	2.90	3.21	3.63	2.18
Clad Damage (dpa)	97	214	294	1537

The downward trend in transuranics burned per year from the 100 dpa cycle to the once through cycle is caused by the increase in fusion power in the system. ERANOS calculates the total power deposited in the system accounting for both fission events and neutron heating from the fusion neutron source. The drastic decrease in transuranics burned per year from the 200 dpa cycle to the once through cycle is due

to the high fusion powers necessary to maintain the fission reaction.

5.1.1 Power Distribution for the Accumulated Radiation vs Burnup Fuel Cycles

The power distribution in each of the four fuel cycles at BOC and EOC was investigated. The goal is to minimize the power peaking in the system. The maximum allowable radial power peaking was set at a limit of 2.0. Figure 13 shows the radial power distribution at BOC and EOC for each of the four fuel cycles.

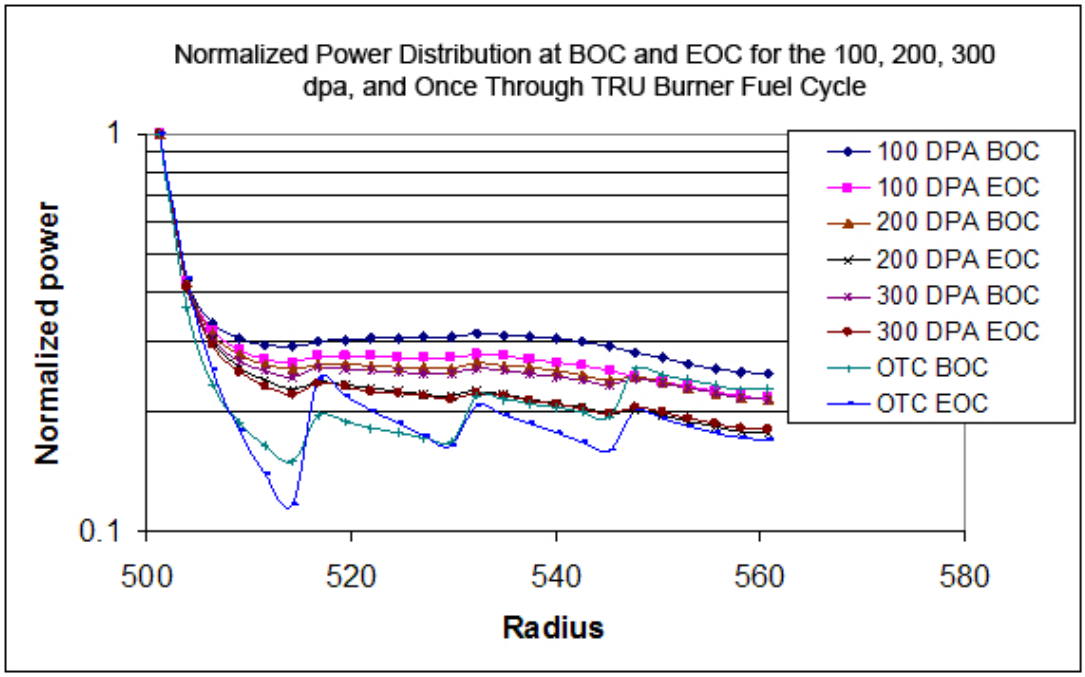

Figure 13: Radial Power Distribution for the TRU Burner Fuel Cycles

For all four fuel cycles the power peaks in the inner most regions of the core. This is caused by the plasma neutron source being located next to the inner most region of the core. The excess neutrons in the inner ring of assemblies are more likely to be fissioned and thus create this large power spike in this region. The recycling and reprocessing cycles follow a very smooth curve from the inner assembly to the outer assembly regions. The opposite is true of the once through cycle. The once through cycle has power discontinuities at each assembly interface. The large power

discontinuities at the interfaces between assemblies in the once through cycle are caused by fresher fuel in the outer assembly having higher macroscopic fission cross sections than in the outer most portion of the inner assembly. These discontinuities are smaller in the reprocessing fuel cycles but are still present.

5.1.2 Repository Effects of the the Accumulated Radiation vs Burnup Fuel Cycles

The decay heat to the repository was calculated via ORIGEN-S [21]. Fast group cross sections were imported into ORIGEN-S and the fuel was then depleted under a constant flux until the burnup reached the same level of burnup seen in ERANOS. The calculation of decay heat to the repository was done assuming reprocessing separations of 1%, meaning 99% of the minor actinides are fed back into the system with 1% in the fission product waste stream. The separation levels are a very conservative assumption. Electrochemical reprocessing has never been done on the industrial scale, only on a laboratory scale. The separation efficiencies in Table 8 have been estimated for Np, Pu, Am, and Zr by Argonne National Laboratory [20]. Table 9 shows the amount of transuranics to the repository for each of the 4 fuel cycles; while Figure 14 shows the decay heat to the repository for each of the four TRU burner fuel cycles as well as a typical light water reactor once through fuel cycle.

Table 8: Recovery Efficiency of Key Elements for Electrochemical Reprocessing [30]

Element	Recovery Efficiency
Plutonium	>99.85%
Neptunium	>99.85%
Americium	>99.97%
Curium	>99.95%

Table 9: Transuranic Waste in Kilograms to the Repository after each Reprocessing Step for SABR

Isotope	100 dpa	200 dpa	300 dpa	Once Through
U235	0.022	0.178	0.20	12.4
U238	3.15e-5	1.04e-4	1.1e-4	8.8e-3
Np237	8.088	4.28	3.28	8.45
Np239	1.47e-6	1.45e-6	1.34e-6	6.75e-5
Pu238	7.21	10.2	9.68	77.1
Pu239	18.05	10.84	8.83	53.1
Pu240	15.13	17.27	16.01	322.7
Pu241	3.32	3.42	3.28	100.8
Pu242	2.99	4.32	4.18	216.3
Am241	7.22	4.41	3.49	19.8
Am242m	0.469	0.49	0.45	2.52
Am243	1.71	1.64	1.50	68.9
Cm242	0.42	0.35	0.30	3.02
Cm243	0.039	0.06	0.07	1.2
Cm244	0.77	1.49	1.51	119.9
Cm245	0.08	0.32	0.36	47.9
Total	65.8	60.2	54.0	1090

For the decay heat calculation all four fuel cycles are compared against each other and the current light water reactor once through fuel cycle. The reprocessing and recycling fuel cycles perform the best in regards to decay heat with the 300 dpa having the smallest long term decay heat to the repository. The reduction in long term decay heat is caused by the reduction in minor actinides being stored in the

repository.

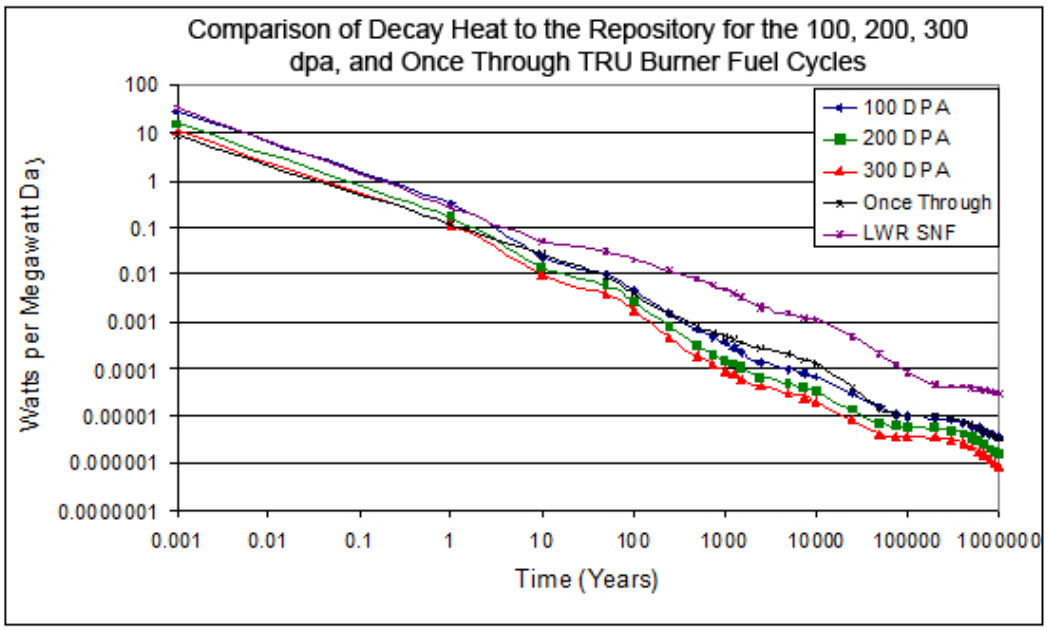

Figure 14: Comparison of Decay Heat to the Repository for Different Fuel Cycle Lengths

The decrease from 64 kilograms of transuranics in 100 dpa cycle to 54.0 kilograms in the 300 dpa fuel cycle is slightly deceiving because this is after each reprocessing step. The key metric would be the amount of transuranics to the repository per year, which for the each cycle is 68.62 kg for the 100 dpa cycle, 31.31 kilograms for the 200 dpa cycle, 19.71 kilograms for the 300 dpa cycle and 87.43 kilograms for the once through cycle. From these numbers as well as from the decay heat data it does not appear that there is a large benefit in extending the fuel cycle beyond the current irradiation damage limit of 200 DPA. Thus the 200 DPA fuel cycle is the benchmarked fuel cycle.

5.2 TRU Burner Fuel Cycle

The initial calculations for fuel residence versus radiation damage were done assuming a fuel smear density of 100% and no rotation of fuel assemblies with shuffling, i.e. the same face of the assembly would be located inboard as the assembly was shuffled from the outmost to the innermost ring over the fuel cycle. The calculations on the reference 200 dpa cycle were repeated to investigate the effect of i) utilizing a smear density of 95% in order to accommodate fuel swelling and expansion, and ii) of rotating the fuel assemblies by 180^o each time they were shuffled. The simulation was run for 700 days; as was previously done so that the results of the reduction of smear densities could be compared. The model was changed such that each fuel assembly has been split into two components to facilitate the rotation of the fuel at the end of each batch time.

5.2.1 Radiation Damage Benefits of Fuel Rotation

The first thing investigated was the DPA that occurred in each half of the fuel assemblies as a function of time. The DPA accumulated in each radial assembly over a batch time would reveal what rotation pattern is the most effective in reducing the maximum radiation damage to the system. The graph of DPA accumulation in each region by batch is shown in Figure 15 below.

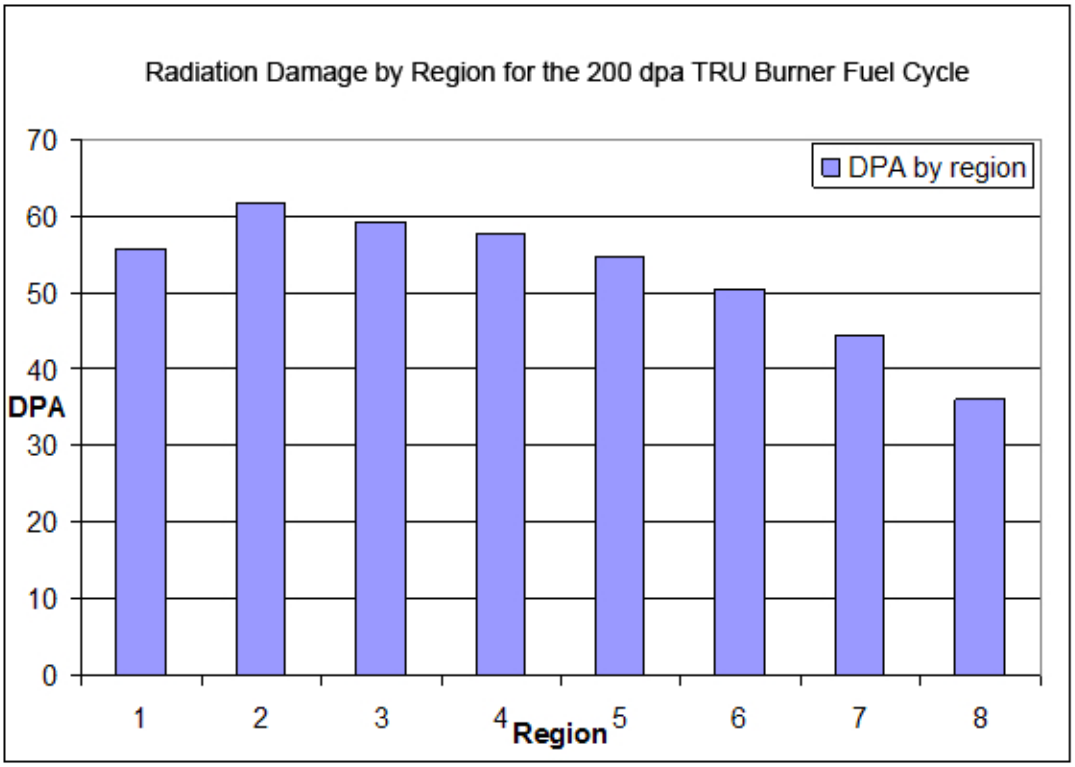

Figure 15: Radiation Damage by Region for the 200 dpa TRU Burner Fuel Cycle

The damage profile can be explained by the neutron flux spectrum in the system. Figure 16 shows the neutron flux as a function of space and energy.

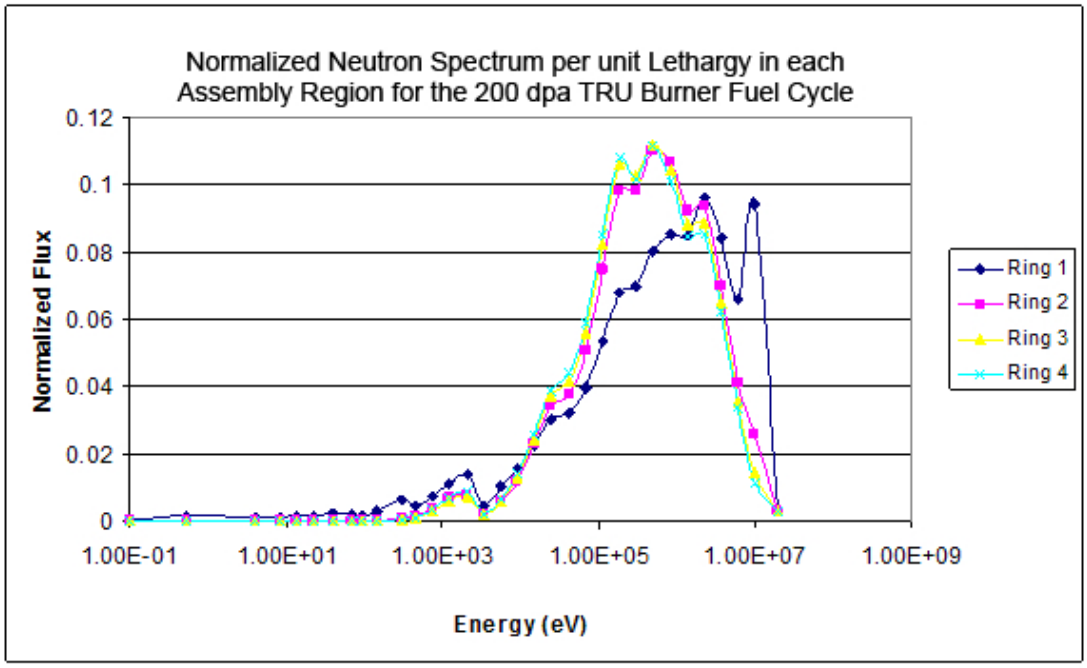

Figure 16: Flux Spectrum by Ring for the 200 dpa TRU Burner Fuel Cycle

The greater number of both low energy neutrons and 14 MeV neutrons in the innermost fuel ring is caused by the fusion neutrons; the low energy neutrons are being reflected back into the core through the tritium breeding blankets on the inboard side of the plasma as well as through the tritium breeding blankets on the top and bottom of the plasma. The greater number of 14 MeV neutrons are from direct streaming of the fusion neutron source into the fission core. The fusion neutrons have lost energy via elastic collision by the time they reach the outer most fuel rings. The rise in dpa from region 1 to region 2 is due to the mean free path of a fusion neutron is approximately 10 cm and this is in region two lending to a harder neutron spectrum in this region than in region 1 and a smaller influence of the reflected neutrons from the tritium breeding blankets. The radiation damage as a function of neutron energy and space is shown in the Figure 17.

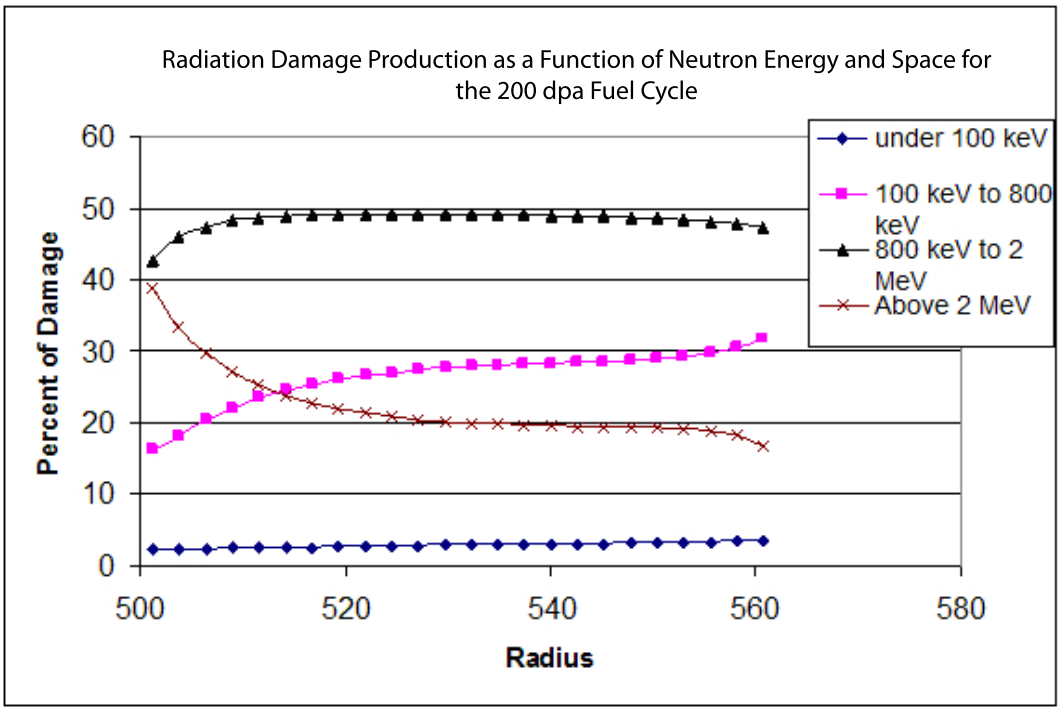

Figure 17: Radiation Damage Production as a Function of Energy, for the 200 dpa TRU Burner Fuel Cycle

The above 2 MeV line on the graph refers to the contribution of the fusion neutron source. It was assumed the fission neutrons would be born with energy less than 2 MeV, therefore all neutrons with energy above 2 MeV were born from the D-T fusion reaction and have slowed down from 14.1 MeV to 2 MeV. The contribution of the neutrons in the range between 2 and 14 MeV are more significant in the first assembly region, accounting for between 25% and 38% of the radiation damage. Where in the rest of the core it is approximately 20% throughout. From the information contained in Figures 16 and 17, radiation damage per region and radiation damage as a function of energy, the rotation pattern was chosen by minimizing the accumulated radiation damage in each zone at each time step. Utilizing this method, the rotation pattern that minimized radiation damage is as follows: the fuel in regions 7 and 8 (outermost

ring of fuel assemblies) is rotated 180 degrees and placed in regions 6 and 5 respectively. The fuel in regions 5 and 6 (the third ring of fuel assemblies) is not rotated and translated into regions 3 and 4 respectively. The second ring of fuel assemblies (regions 3 and 4) is rotated and shifted one assembly inward to regions 2 and 1. This reduces the accumulated DPA to 212 from 218. The resulting fuel cycle is shown in Figure 18. Figure 19 is the accumulated radiation damage versus region for the rotated fuel cycle.

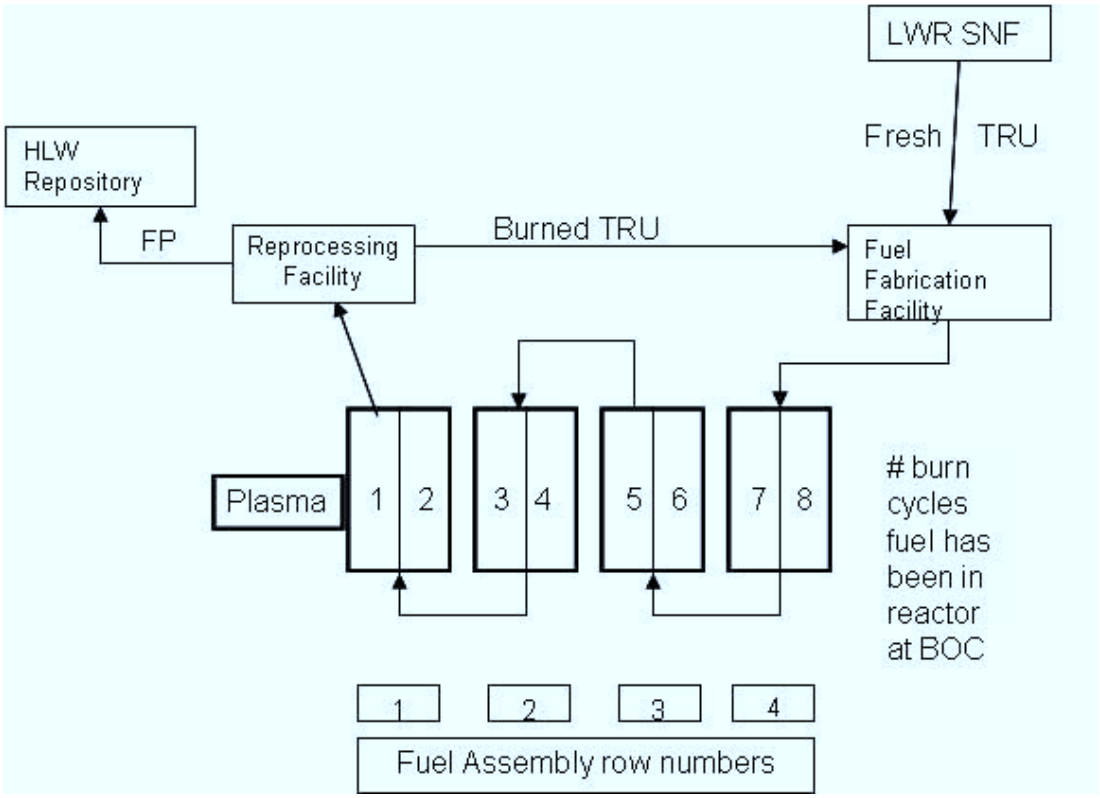

Figure 18: Rotation Pattern for SABR Fuel Cycle

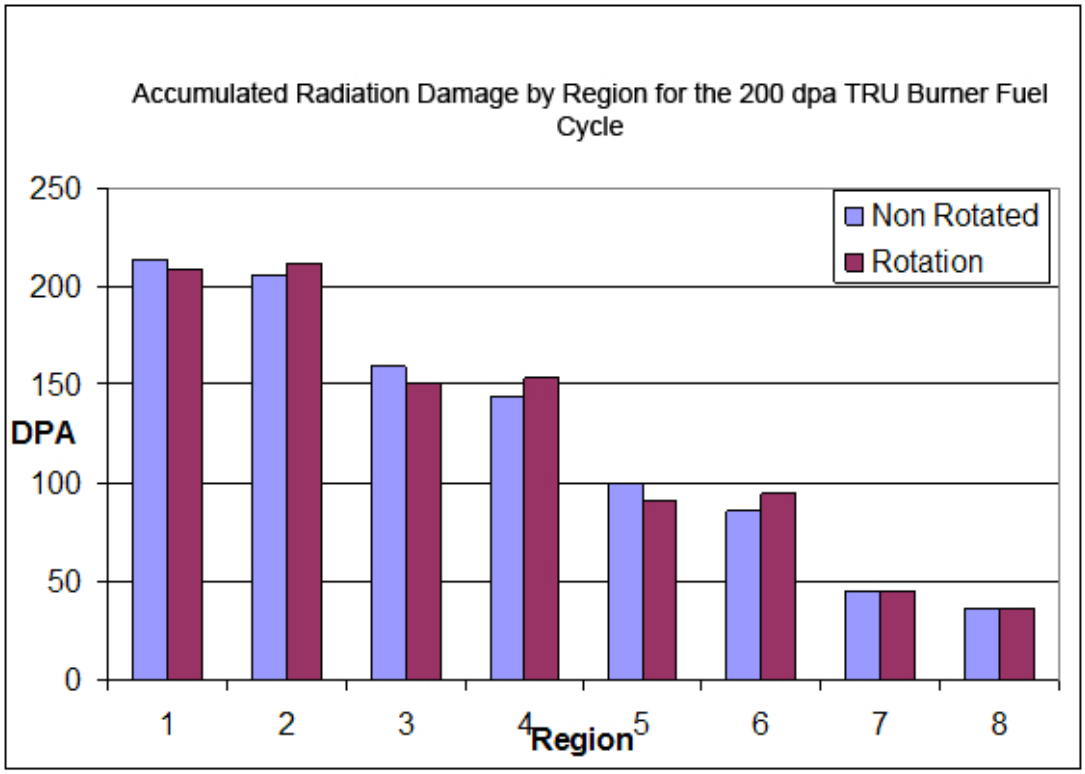

Figure 19: Accumulated Radiation Damage versus Region for the 200 dpa TRU Burner Fuel Cycle

5.2.2 Power Profiles for the 200 dpa Rotated TRU Burner Fuel Cycle

Rotation of the fuel assemblies has an impact on the radial power distribution in the fuel assemblies. The resulting power profile from the change to rotated assemblies as well as the power generated in each half assembly is shown in Figures 20 and 21.

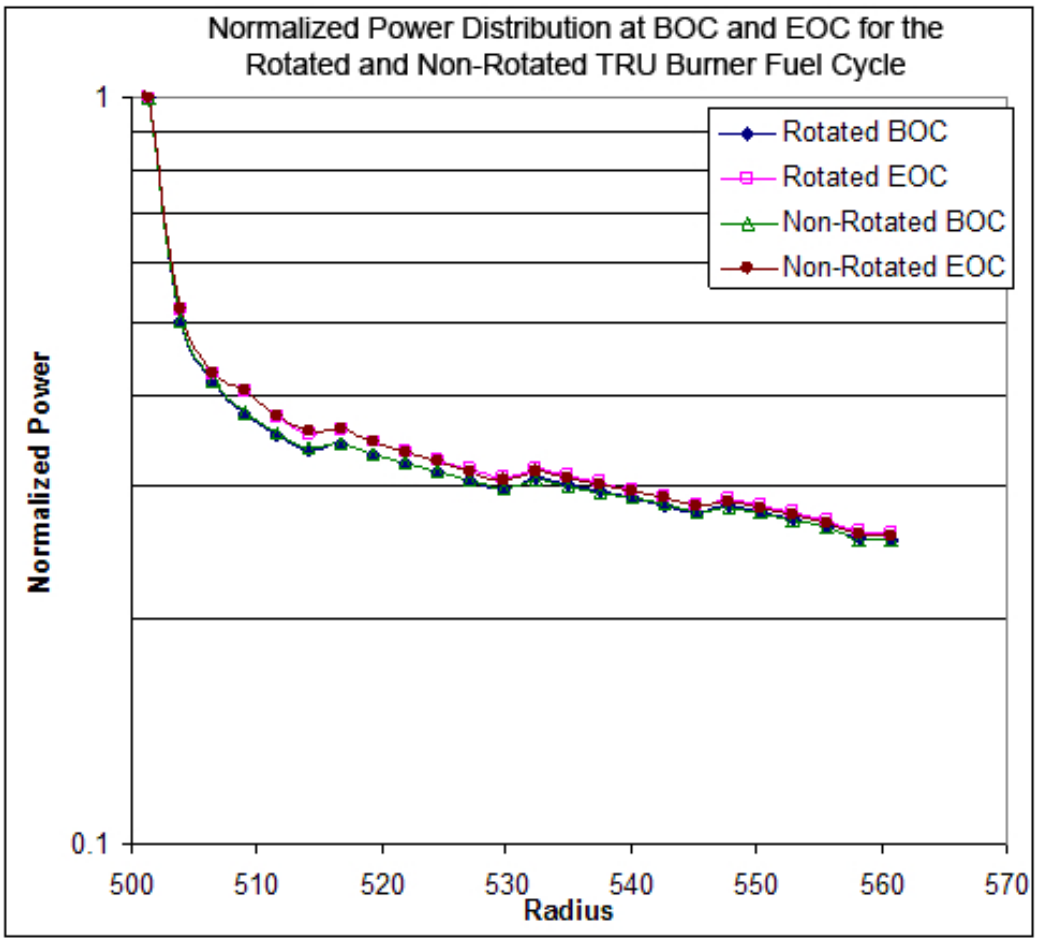

Figure 20: Power Distribution for 200 dpa TRU Burner Fuel Cycle

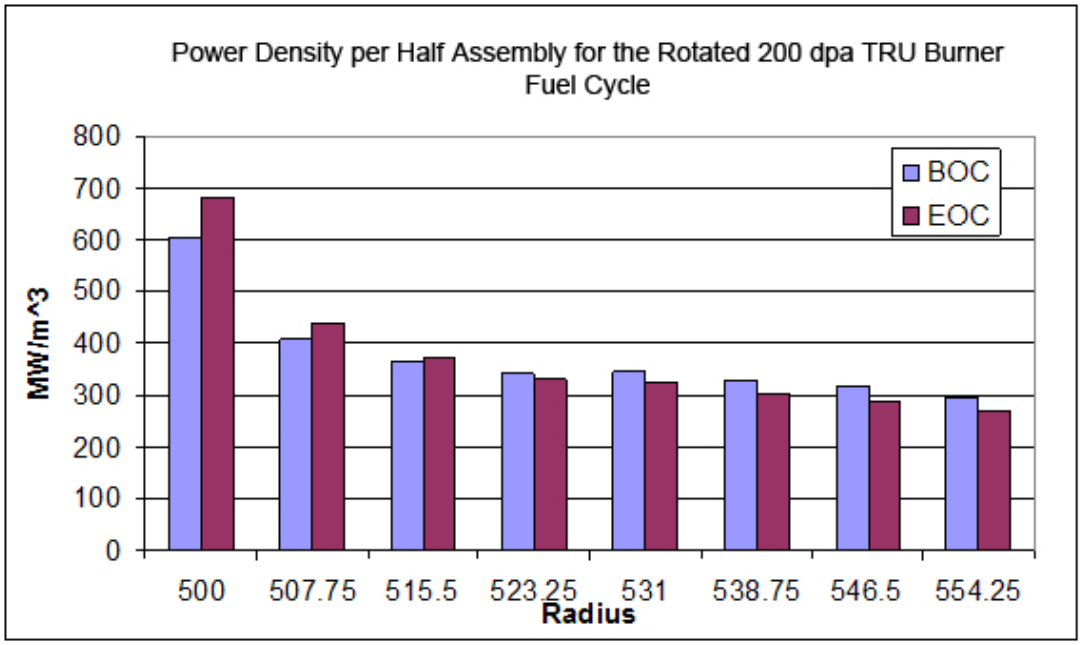

Figure 21: Power Density per Half Assembly for the 200 dpa TRU Burner Fuel Cycle

The regional power peaking is 3% smaller for the rotated fuel assemblies than for the non rotated fuel assemblies. The overall radial power peaking is much larger due to the large power spike closest to the plasma. The large power spike in the innermost region of the fission core is due to neutrons being thermalized by the inner tritium breeding blanket and being reflected back into the fission core. This softer flux spectrum is seen in Figure 16, flux spectrum by ring for the 200 dpa TRU burner fuel cycle. To confirm that the softer spectrum is being caused by thermal neutrons reflecting into the core from the inner tritium breeding blanket, a simulation was run with the inner breeding blanket being removed. The effect of the removal of the tritium breeding blanket is shown in Figures 22 through 25.

The large difference in the number of fissions occurring from neutrons less than 8 eV, 60% for the original configuration as compared to 40% with the blankets removed. As well as the difference in percentage of power produced from 14% to 8% without the blankets confirms the theory that reflection of neutrons back into the system from the

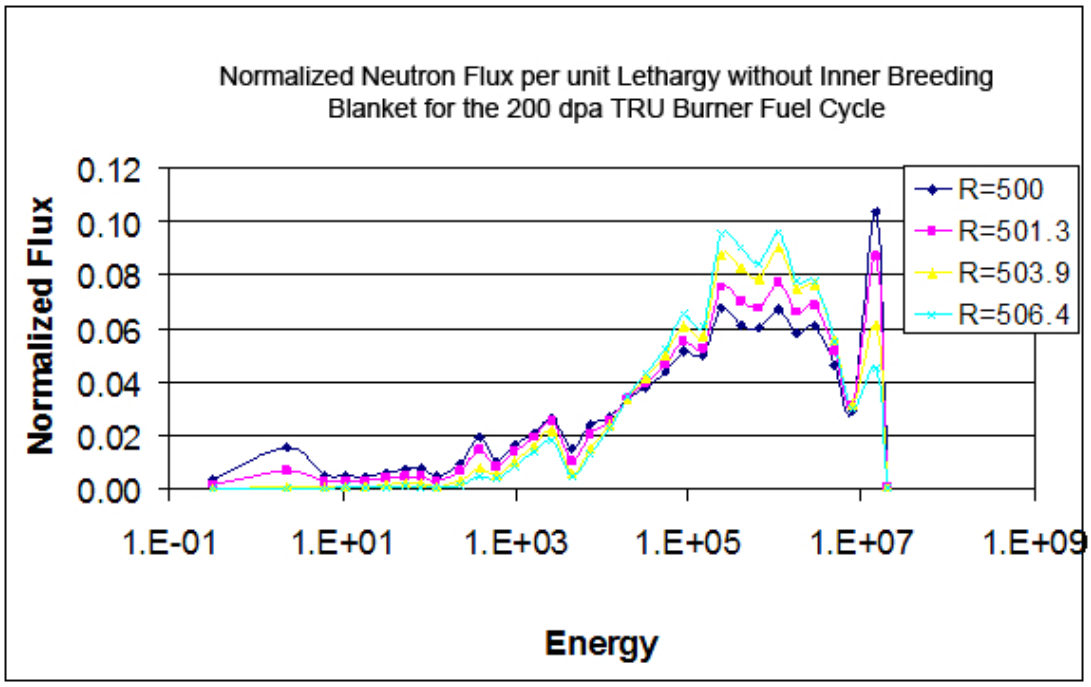

Figure 22: Flux Spectrum by Ring for the 200 dpa TRU burner Fuel Cycle without the Inner Tritium Breeding Blanket

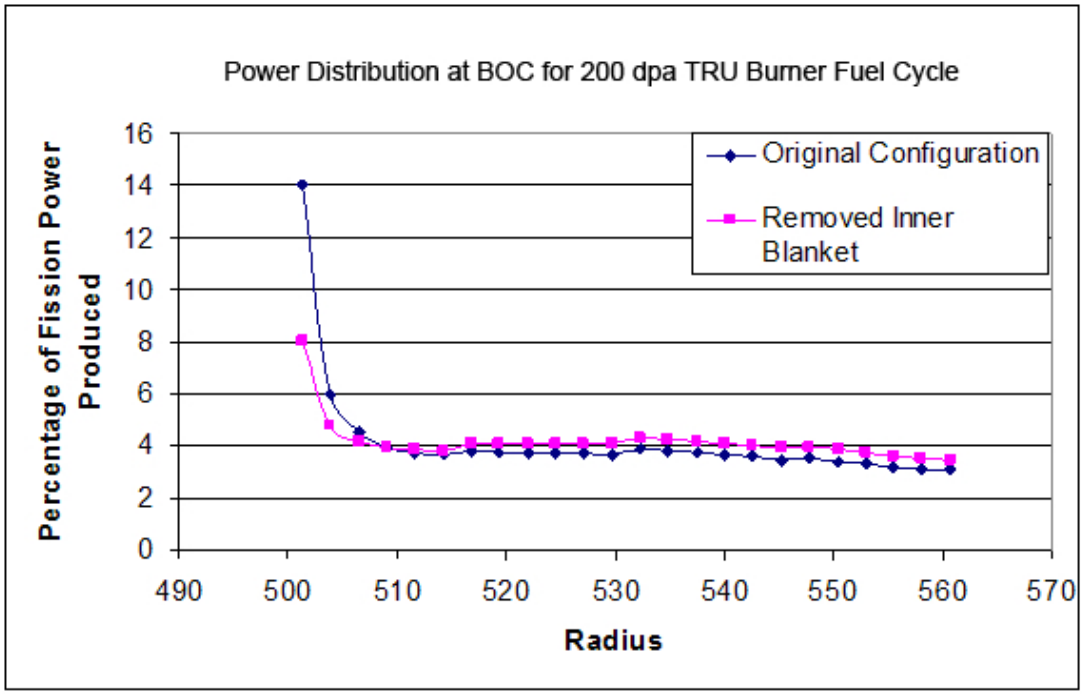

Figure 23: Radial Power Distribution Comparison for the 200 dpa TRU Burner Fuel Cycle with and without the Inner Tritium Breeding Blanket

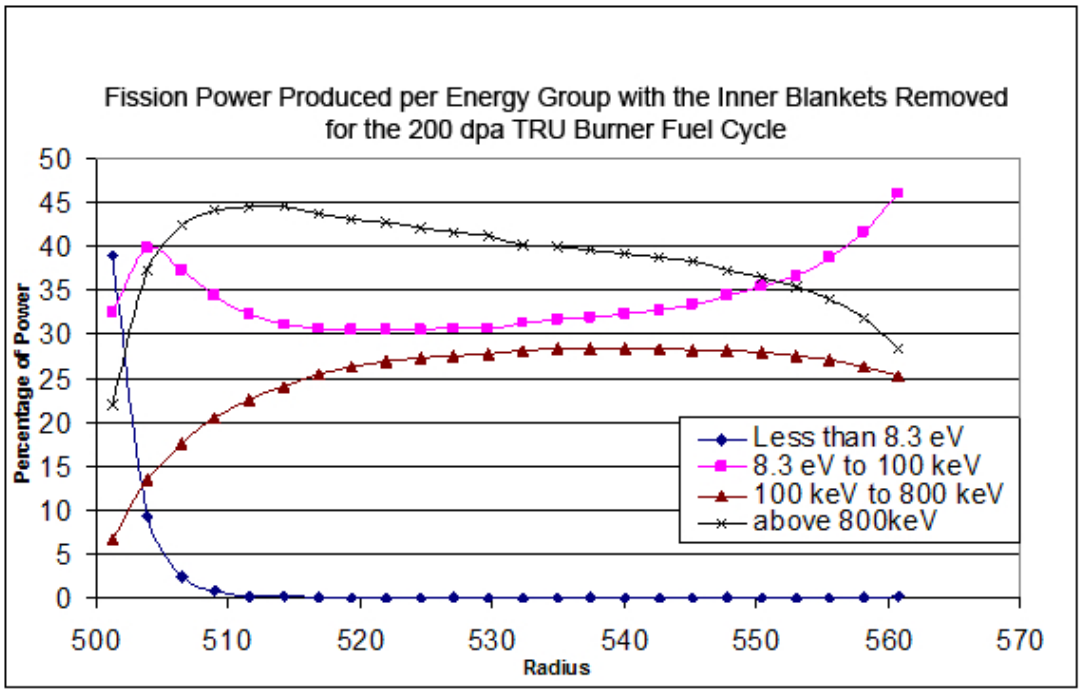

Figure 24: Fission Power Produced by Neutrons in Different Energy Ranges for the 200 dpa TRU Burner Fuel Cycle without the Inner Tritium Breeding Blanket 200

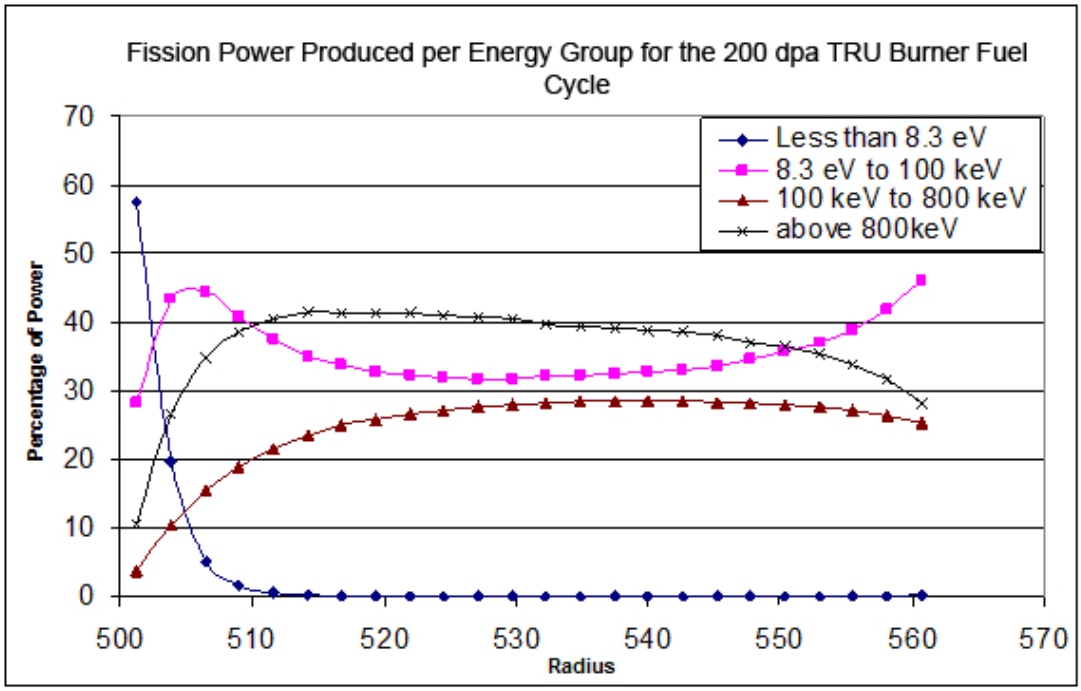

Figure 25: Fission Power Produced by Neutrons in Different Energy Ranges for the 200 dpa TRU Burner Fuel Cycle

inner tritium breeding blanket is causing the softer and spectrum and the power spike near the first wall. To account for the power spike generated by the slowing down of fusion neutrons and a softer flux spectrum the sodium flow will be zoned so that the innermost assembly receives a greater mass flow rate than the outer assemblies. This will allow for the outlet temperature of the sodium to be similar at the outlet of each fuel assembly.

The axial power profile is much flatter than the radial power profile. The axial profile is flatter and closer to what would be expected in a critical system. The power discontinuity at both the top and bottom of the system is caused by neutrons being thermalized and reflected back into the fission core from the tritium breeding blanket, and additional neutrons from the fusion neutron source streaming in through the tritium breeding blanket and entering the fission core at lower neutron energies. Figure 26 shows the axial power profile in each of the four fuel assembly regions for the 200 dpa fuel cycle.

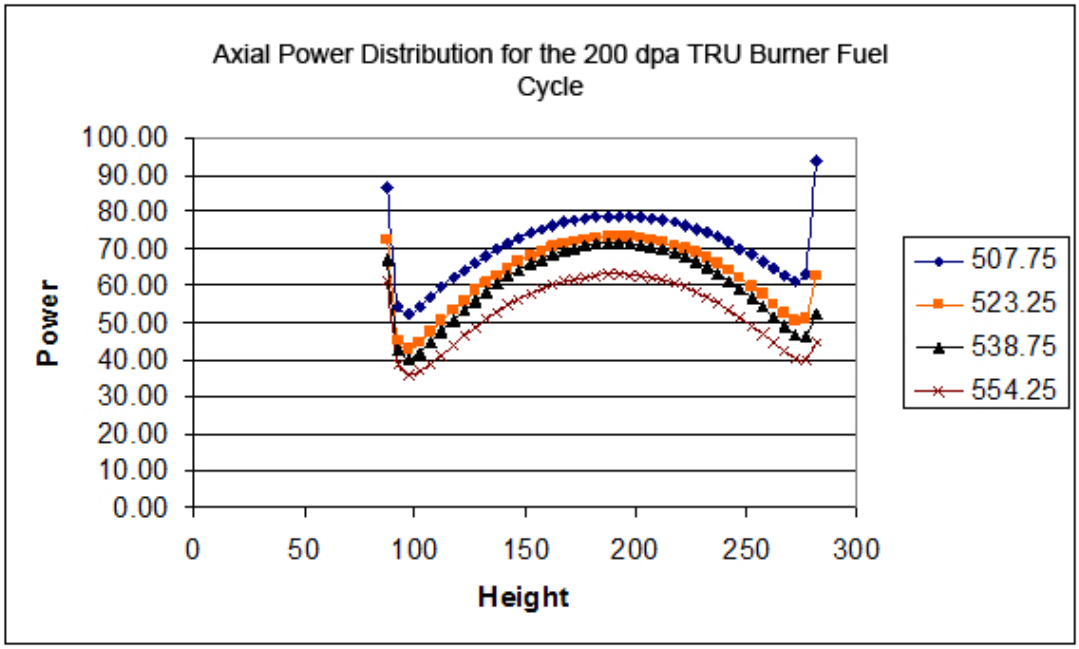

Figure 26: Axial Power Profile in each Assembly Region for the 200 dpa TRU Burner Fuel Cycle

5.2.3 Repository Effects for the Rotated and Non-Rotated TRU Burner Fuel Cycle

The decay heat to the repository is slightly reduced with the lowered smear density, causing less fuel in the reactor at BOL. This slight reduction in fuel at BOL results in fewer kilograms of minor actinides at EOC and thus fewer kilograms to the repository while maintaining a similar support ratio. Figure 27 displays the decay heat for the rotated, non-rotated, and a representative light water reactor.

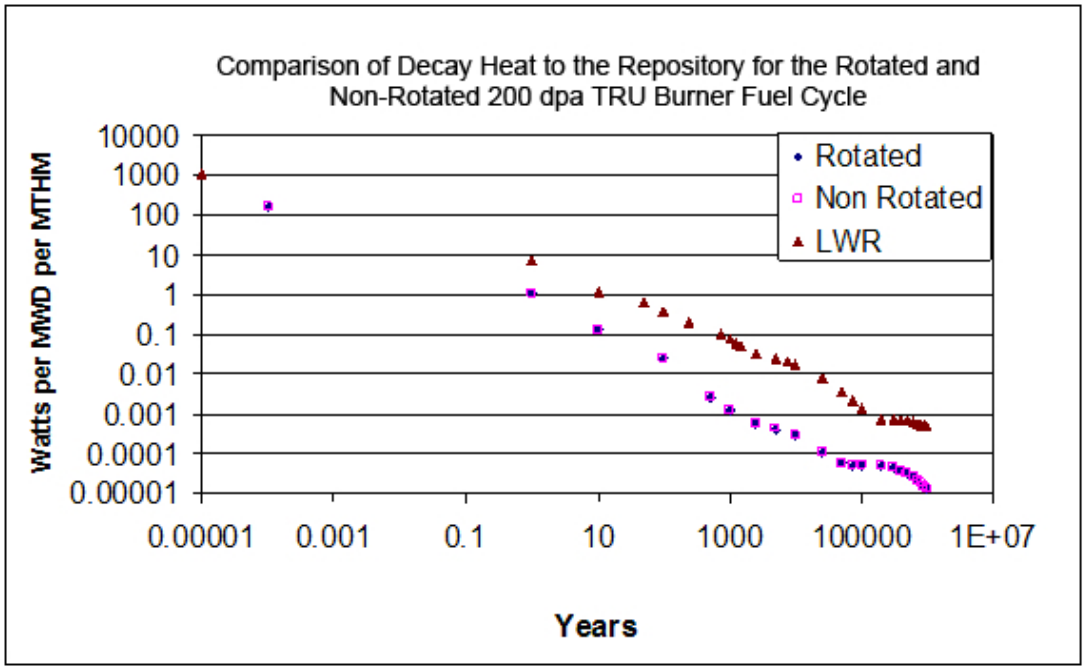

Figure 27: Decay heat to the repository for the Rotated and Non-Rotated 200 dpa Fuel Cycle

This reduction in decay heat also reduces the need for repository space. Equation 10 illustrates between the integral decay heat produced per MW_d per MTHM in SABR, W_{SABR}, and the integral decay heat produced per MW_d in a typical LWR, W_{LWR}. This relationship can be used to determine the reduction in necessary repository space that SABR provides.

$$F = \frac{W_{SABR}}{W_{LWR}} \tag{10}$$

The integration of the decay heat is done out to 100,000 years. The reduction in necessary repository space is not extremely large. With the assumption of constant nuclear spent fuel production of 2,000 MT, per year this reduces the effective repository space needed by a factor of 10.37 for the rotated case, and 10.29 for the non-rotated case as compared to 10.06 for the case of 100% smear density.

5.2.4 Tritium Breeding Gain for the Rotated 200 dpa TRU Burner Fuel Cycle

The net tritium production needs to be calculated in SABR. The tritium production was calculated via ERANOS and the tritium breeding gain was calculated by discretizing equation 2.

$$P_T(t) = \sum_{region} \sum_{I=Li6,Li7} \sum_{g=1}^{27} \phi_{g,region} \sigma_g^I(n,\alpha) N_{region}^I V_{region} \tag{11}$$

In calculating the breeding gain a linearization of Equation 5 is done. This is done in the same manner as was done in a previous study by Maddox [18].

$$\frac{dN}{dt} = [P_{T1} + \frac{(P_{T2} - P_{T1}) \times t}{C_{time}}] - [D_{T1} + \frac{(D_{T2} - D_{T1}) \times t}{C_{time}}] - \lambda N_T(t) \tag{12}$$

P_{T1}, P_{T2}, D_{T1}, and D_{T2} are the beginning and end of cycle tritium production rates and beginning and end of cycle tritium destruction rates respectively, and C_{time} is the length of each fuel cycle batch, 700 days in the 200 dpa fuel cycle. To obtain the amount of tritium at end of cycle equation 12 is solved for N_T(EOC).

$$\begin{aligned} N_T(EOC) &= N_T(0) \times e^{-C_{time} \times \lambda} + \frac{P_{T1} - D_{T1}}{\lambda} \times (1 - e^{-C_{time} \times \lambda}) \\ &+ \frac{P_{T2} - P_{T1} + D_{T1} - D_{T2}}{\lambda^2 \times C_{time}} \times (\lambda \times C_{time} - 1 + e^{-C_{time} \times \lambda}) \end{aligned} \tag{13}$$

When calculating the tritium breeding and therefore the tritium self sufficiency, a 90 day down time was assumed. The down time is the amount of time that occurs between cycles for maintenance and refueling. This is a conservative measure that takes into account problems during refueling since refueling outages should last approximately 30 days. Also the time it takes for the online gas purging of tritium to become available was estimated and taken into account when making the self sufficiency calculations. The amount of tritium needed at the beginning of the cycle is dependent on the fusion power level (TRU destruction rate) at BOC and EOC, the cycle length, and the lead time. The *leadtime* is the amount of time it takes for

tritium from the online purge system to become available.

$$N_T(0) = [D_{T1} + \frac{D_{T2} - D_{T1} \times leadtime}{2 \times C_{time}}] \times leadtime \tag{14}$$

Determining if their is enough tritium at the beginning of cycle the amount of tritium at end of cycle is decayed for the 90 day downtime.

$$N_T(0') = N_T(EOC) \times e^{-\lambda \times downtime} \tag{15}$$

There is enough tritium in the system if after the decay time the amount of tritium present in the system is greater than the amount required at BOC.

$$N_T(0') \geq N_T(0) \tag{16}$$

Table 10: Tritium Production for the 200 dpa TRU Burner Fuel Cycle

	200 dpa Rotated	200 dpa Non-Rotated
BOC Tritium Destruction	1.07e20	1.12e20
BOC Tritium Production	1.26e20	5.72e20
EOC Tritium Destruction	1.42e20	1.43e20
EOC Tritium Production	2.03e20	8.76e20
Tritium Necessary for BOC	9.84e21	1.03e22
Tritium at BOC	1.12e22	1.18e22

Table 11: TRU Burner 200 dpa Rotated and Non-Rotated Fuel Cycle Results

	200 dpa Rotated	200 dpa Non-rotated
Fission Power (MW_{th})	3000	3000
BOL Mass HM (kg)	30254	30254
BOC Mass HM (kg)	28846	28849
EOC Mass HM (kg)	26803	26809
Delta Mass (kg)	2042	2040
Loading Outer (kg)	7887	7887
HM out (kg)	5845	5847
FIMA (%)	25.6	25.6
Regional Power Peaking Radial BOC/EOC	1.66/1.89	1.69/1.93
BOL P_{fus} (MW)	172	172
BOC P_{fus} (MW)	302	317
EOC P_{fus} (MW)	401	429
BOL k_{eff}	0.945	0.945
BOC k_{eff}	0.878	0.863
EOC k_{eff}	0.831	0.817
Cycle Reactivity Change	-6441 pcm	-6526 pcm
TRU Burned/yr (kg)	1027	1023
MA Burned/yr (kg)	342	341
Pu Burned/yr (kg)	685	684
U Generated/yr (kg)	0.5	0.5
Support Ratio (100%)	4.2	4.2
Support Ratio (75%)	3.2	3.2
Clad Damage (dpa)	212	218

Table 11 summarizes the comparison of the rotated and non-rotated 200 dpa TRU burning fuel cycles. The rotated fuel cycle burns slightly more transuranics per year with less damage to the cladding than the non-rotated fuel cycle. The 3% reduction in dpa by rotating the fuel does not appear to be a large gain, but the fusion power is higher in the rotated case resulting in more high energy neutrons in the system and a harder spectrum, this harder spectrum is more damaging and thus the rotation of the fuel assemblies results in a much larger improvement than the reported 3%. The rotation of the fuel assemblies also reduces the power peaking by approximately 2% at both BOC and EOC with a larger fusion source, if the source would have remained the same the reduction in power peaking would have been greater. The slightly smaller fusion power required for the rotated fuel cycle resuls in less external heating being necessary and increase the overall efficiency of the system. Overall the performance of the two fuel cycles is very similar with the rotated version resulting in a slightly better performance than the non-rotated fuel cycle. The BOC and EOC fuel compositions as well as the amount of transuranics and fission products to fuel fabrication and geological repository are shown in Table 12.

Table 12: SABR Fuel Compositions at BOC and EOC for the TRU Burning Fuel Cycles (weight percent)

Isotope	TRU-Rotate BOC	TRU-Rotate EOC	TRU-Non-Rotate BOC	TRU-Non-Rotate EOC
U234	1.384	1.511	1.383	1.510
U235	0.317	0.351	0.315	0.349
U236	0.119	0.138	0.119	0.139
U238	0.0002	0.0002	0.0002	0.0002
Np237	7.744	6.819	7.746	6.821
Np239	2.269e-6	2.395e-6	2.269e-6	2.395e-5
Pu238	13.528	14.004	13.527	14.003
Pu239	19.391	16.922	19.390	16.921
Pu240	26.362	26.035	26.360	26.033
Pu241	5.475	5.365	5.477	5.367
Pu242	6.809	7.131	6.807	7.128
Am241	7.811	7.063	7.809	7.062
Am242m	0.610	0.588	0.611	0.590
Am243	2.787	2.723	2.786	2.721
Cm242	0.301	0.300	0.303	0.302
Cm243	0.075	0.076	0.072	0.073
Cm244	2.195	2.256	2.198	2.258
Cm245	0.516	0.576	0.517	0.577
Fission Products	4.573	8.148	4.572	8.147

Table 13: SABR Content to the Repository and Fuel Fabrication for the MA Burning Fuel Cycles (kg)

Isotope	TRU-Rotate Repository	TRU-Rotate Fuel Fabrication	TRU-Non-Rotate Repository	TRU-Non-Rotate Fuel Fabrication
U234	1.100	108.923	1.099	108.934
U235	0.278	27.620	0.278	27.623
U236	0.109	10.855	0.109	10.856
U238	0.0001	0.0015	0.0001	0.0015
Np237	3.512	347.603	3.512	347.638
Np239	1.605e-6	1.589e-6	1.605e-6	1.589e-5
Pu238	10.318	1021.523	10.317	1021.625
Pu239	8.489	840.409	8.489	840.493
Pu240	17.139	1696.796	17.138	1696.966
Pu241	3.906	386.582	3.906	386.621
Pu242	5.261	520.84	5.260	520.892
Am241	3.672	363.549	3.672	363.585
Am242m	0.323	31.966	0.323	31.969
Am243	1.753	137.569	1.753	137.583
Cm242	0.325	32.187	0.325	32.190
Cm243	0.063	6.250	0.063	6.251
Cm244	1.597	158.099	1.597	158.115
Cm245	0.498	49.289	0.498	49.294
Total TRU	58.346	5776.23	58.430	5776.81
Fission Products	1030.794	10.412	1030.691	10.413

5.3 Minor Actinide Burner

The next fuel cycles analyzed were for the MA Burning fuel. The design of the MA Burning fuel emphasized on fissioning the minor actinides (MA) in spent fuel while setting aside the plutonium for other uses, as specified in the European studies of reactors to burn minor actinides. The same 200 dpa, 4-batch with rotated-assembly fuel cycle described above was analyzed for both the MA-Oxide and MA-Metallic fuel, fuel cycles. The fuel cycles were evaluated on the same criteria as the TRU burner fuel cycle. Table 14 is a comparison of the metallic and oxide minor actinide burning fuels.

Table 14: MA Burner Metallic and Oxide Fuel Cycle Results

	MA Burner EFIT-Metal Fuel	MA Burner EFIT-Oxide Fuel
Fission Power (MW_{th})	3000	3000
BOL Mass HM (kg)	49985	47359
BOC Mass HM (kg)	48468	45658
EOC Mass HM (kg)	46441	43542
Delta Mass (kg)	2027	2110
Loading Outer (kg)	13040	12345
HM out (kg)	11013	10234
FIMA (%)	15.5	17.1
Regional Power Peaking Radial BOC/EOC	1.46/1.62	1.34/1.51
BOL P_{fus} (MW)	489	515
BOC P_{fus} (MW)	190	195
EOC P_{fus} (MW)	246	325
BOL k_{eff}	0.889	0.909
BOC k_{eff}	0.949	0.959
EOC k_{eff}	0.932	0.936
Cycle Reactivity Change	-1922 pcm	-2552 pcm
TRU Burned/yr (kg)	1089	1122
MA Burned/yr (kg)	853	674
Pu Burned/yr (kg)	236	469
U Generated/yr (kg)	31	21
Support Ratio (100%)	34.1	27.0
Support Ratio (75%)	25.6	20.2
Clad Damage (dpa)	203	201

The change in reactivity throughout the fuel cycle is greater in the oxide fuel than the metallic fuel because more plutonium is burned. This results in a greater change in fusion power from beginning of cycle to end of cycle. The fusion power required to maintain 3000MW$_{th}$ fission power varied from 200 to 500 MW in this fuel cycle, and the rate of MA destruction was 850 and 675 kg/EFPY, for metal and oxide forms of the fast reactor fuel, respectively. The transuranic transmutation rate for the EFIT fuel is 1089 kg per year for the metal and 1122 kg per year for the oxide fuel. The metal fuel burns more minor actinides than the oxide fuel; 78.3% of the transuranics burned in the metal fuel is minor actinides compared to 58.9% of the transuranics burned in the oxide fuel. The metal fuel is in a harder spectrum, making the fission cross section of the minor actinides more competitive with the fission cross section of the plutonium in the system. The harder spectrum is a result of the metallic fuel having a somewhat different fuel assembly design with less coolant per assembly. Figure 28 shows the normalized flux spectra for the oxide and metal fuel.

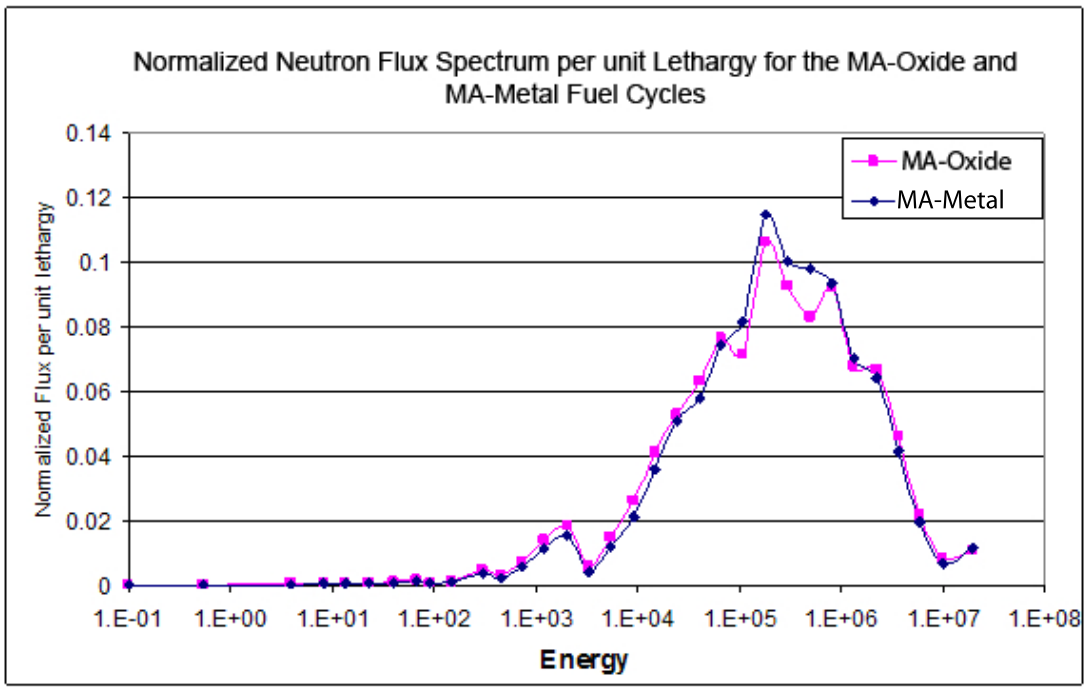

Figure 28: Normalized Neutron Flux Spectrum for the Minor Actinide Oxide and Metallic Fuel

The harder spectrum is a result of the minor actinide fuel having a tighter lattice and less coolant per fuel pin. There is a larger percentage of MgO in the metallic fuel, 60% by volume versus 45% by volume for the metallic to oxide fuel, which would tend to soften the spectrum in the metallic fuel. This factor is dwarfed by the coolant per pin resulting in a harder spectrum for the metallic fuel.

5.3.1 Radiation Damage in the Metallic and Oxide Minor Actinide Burning Fuel Cycles

The harder spectrum in the metallic fuel results in slightly higher accumulated radiation damage for the metallic fuel as compared to the oxide fuel, 203 dpa and 201 dpa respectively. The higher fusion power in the oxide case results in greater radiation damage in the inner most fuel assembly as compared to the metallic fuel. The higher fusion power in the oxide fuel is caused by the fuel having a lower k_{inf} in

the innermost region. This lower k_{inf} results in more of the fusion neutrons being parasitically absorbed instead of fissioning in the innermost assembly as compared to the metallic fuel. The more coolant per pin slows the neutrons causing less damage in the outer assemblies. The radiation damage per assembly and the accumulated radiation damage are shown in Figures 29 and 30 below as well as the neutron spectra in each ring.

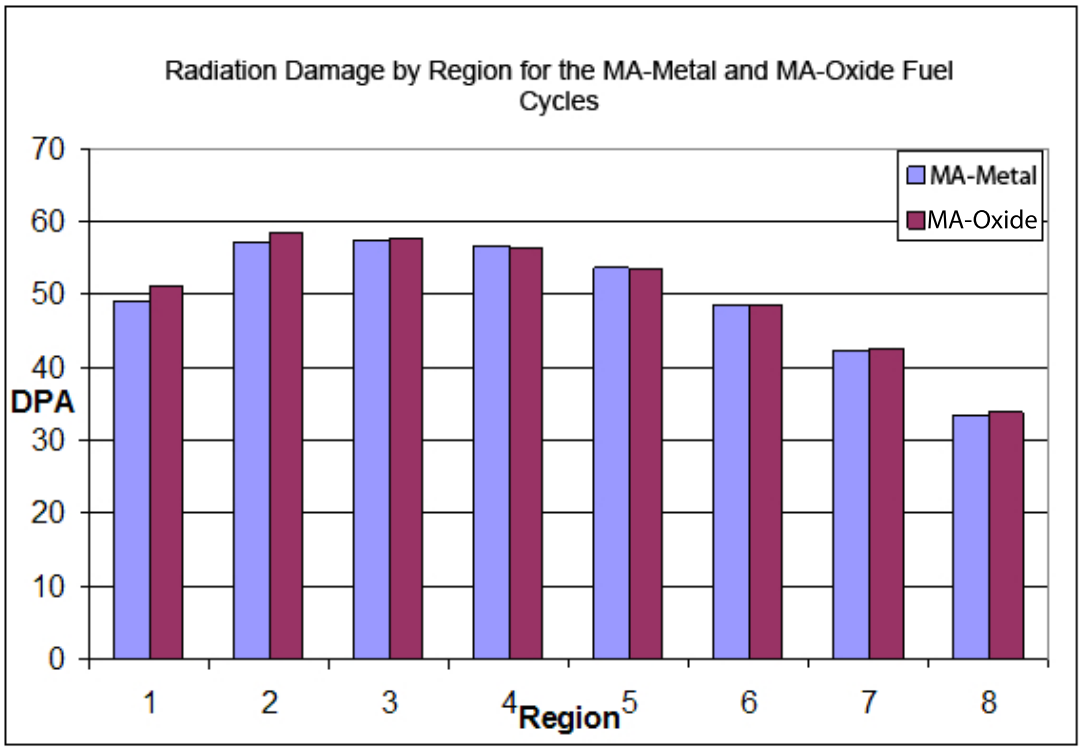

Figure 29: Radiation Damage by region for the Minor Actinide Burning Fuel Cycles

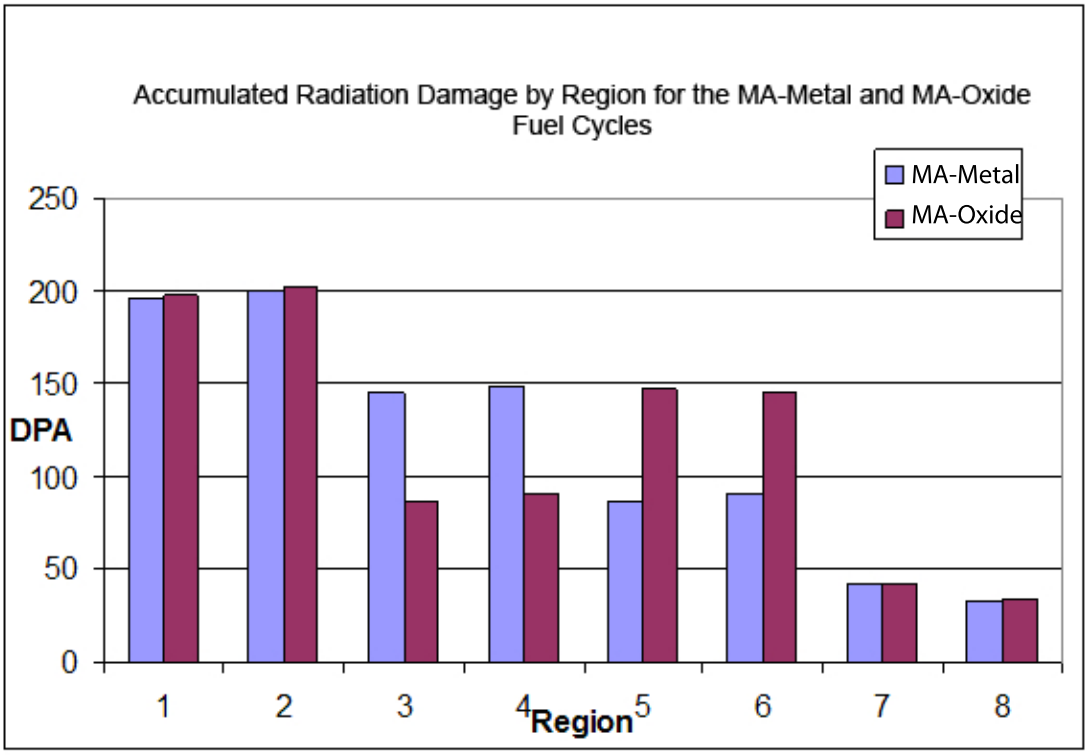

Figure 30: Accumulated Radiation Damage by Region for the Metallic and Oxide Fuel Cycles

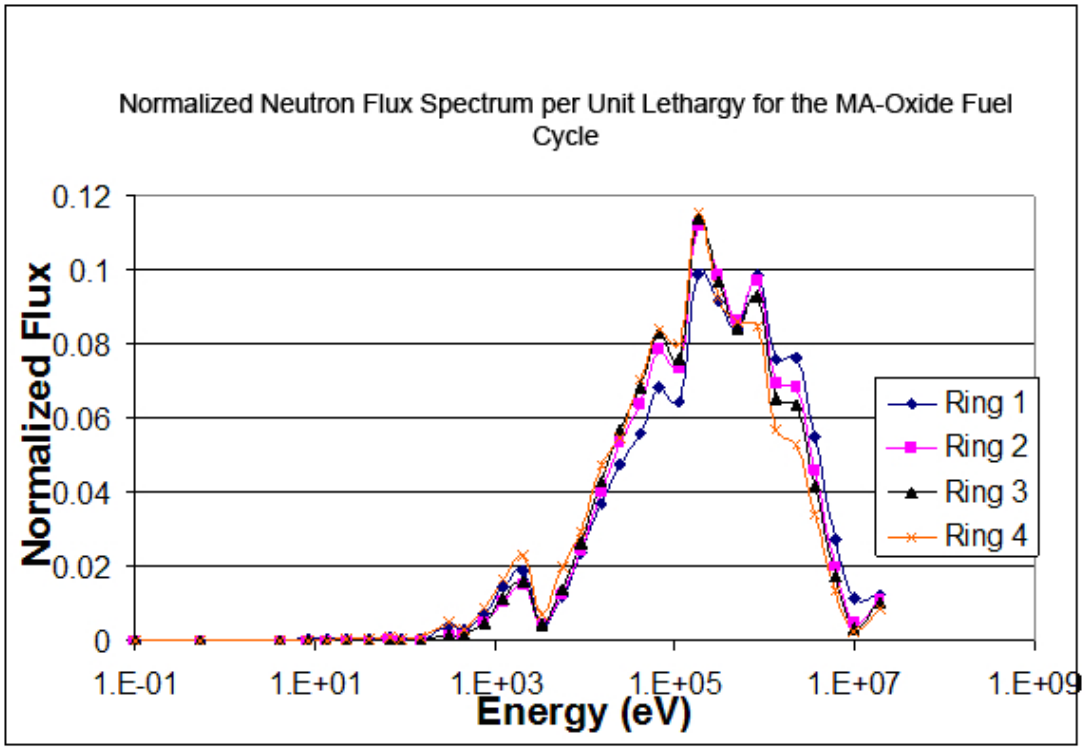

Figure 31: Neutron Spectra by Ring for the MA-Oxide Fuel Cycle

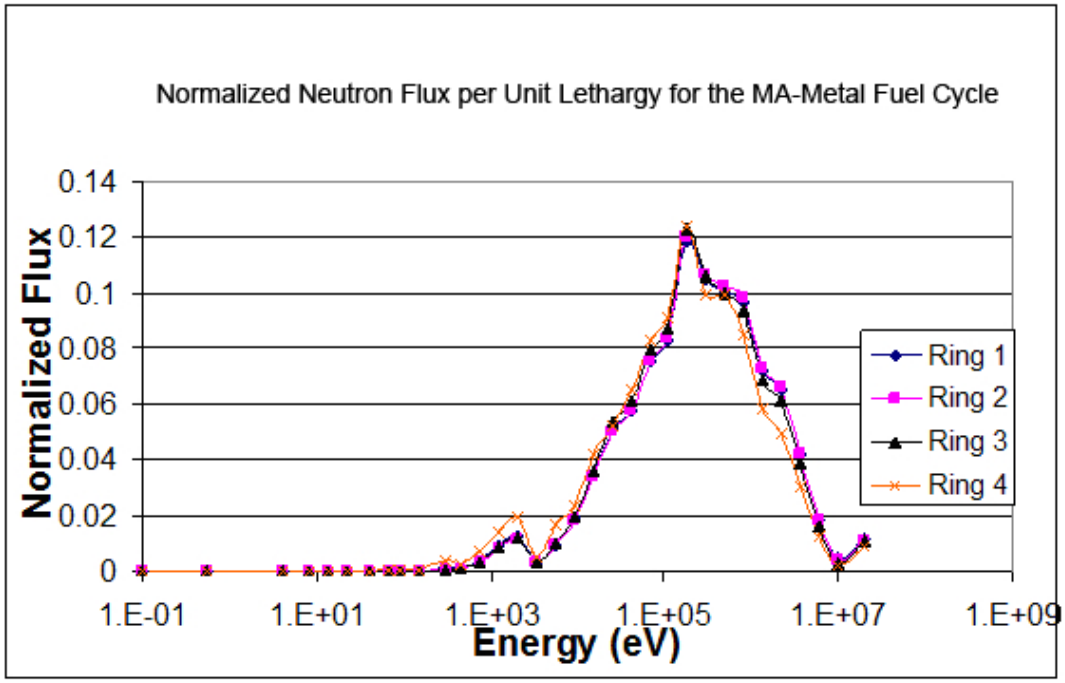

Figure 32: Neutron Spectra by Ring for the MA-Metal Fuel Cycle

From the neutron spectrum of the oxide and metallic fuel cycles and the neutron intensity, the radiation damage as a function of energy and space can be found for both fuel types. Figures 33 and 34 show the radiation damage as a function of space and energy for both the MA-Oxide fuel and MA-Metal fuel.

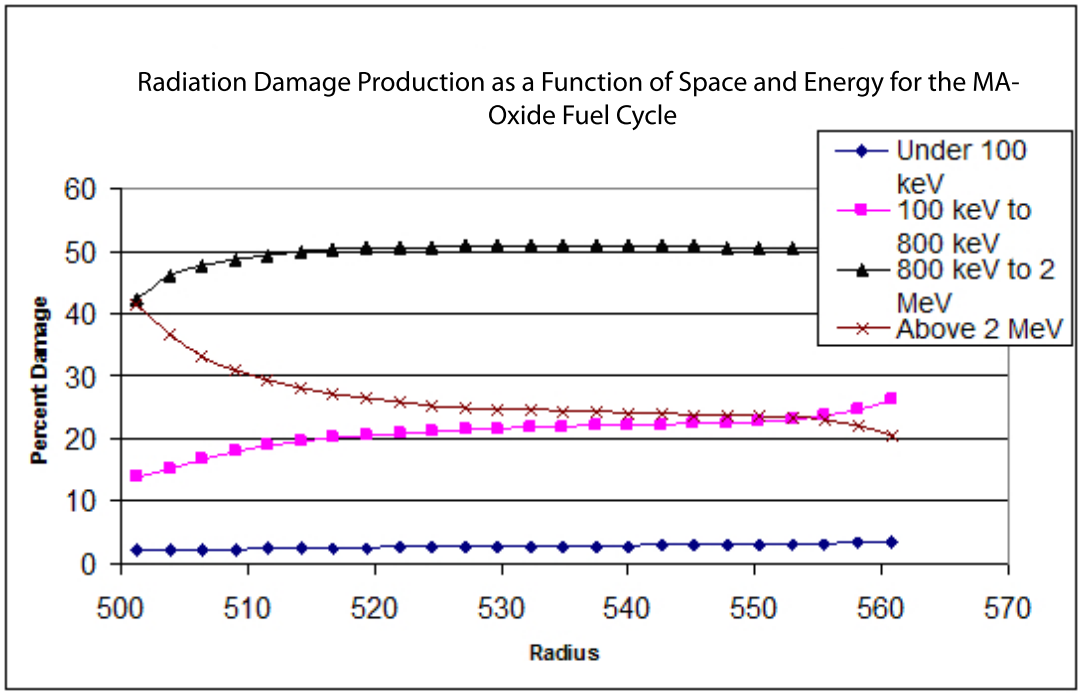

Figure 33: MA-Oxide Radiation Damage Production as a Function of Space and Energy

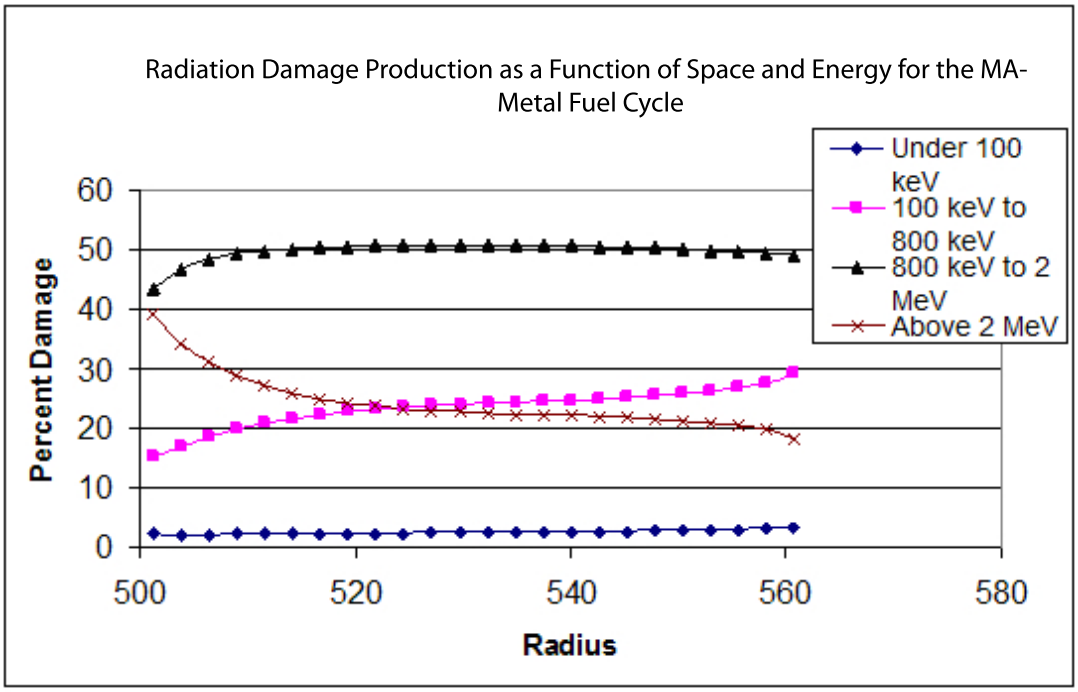

Figure 34: MA-Metal Radiation Damage Production as a Function of Space and Energy

The figures show that the radiation damage is primarily caused by the fission neutrons as well as the slowing down of fusion neutrons in both fuel types. The contribution of fast neutrons, neutrons with energy of greater than 100 keV, to the damage is approximately 97%. In the innermost ring 42% of the damage is caused by fusion neutrons in the oxide fuel and 38% in the metallic fuel. The slight increase in damage from fusion neutrons in the oxide fuel is due to the higher fusion power required to operate the reactor at 3000 MW_{th}. The contribution to radiation damage of the fusion neutrons can also be seen in the spectra plots with the innermost fuel ring having the greatest quantity of high energy neutrons (fission plus fusion).

5.3.2 Power Profiles for the Metallic and Oxide Minor Actinide Burning Fuel Cycles

The power peaking in the oxide fueled system is slightly less than in the metallic fueled system. This is caused by the k_{inf} in each of the four assembly regions being flatter than in the metal fuel. The flatter k_{inf} profile results in greater neutron multiplication in the outer assembly regions and therefore more fissions and more power generated. Figure 35 shows the power distribution for both minor actinide burning systems.

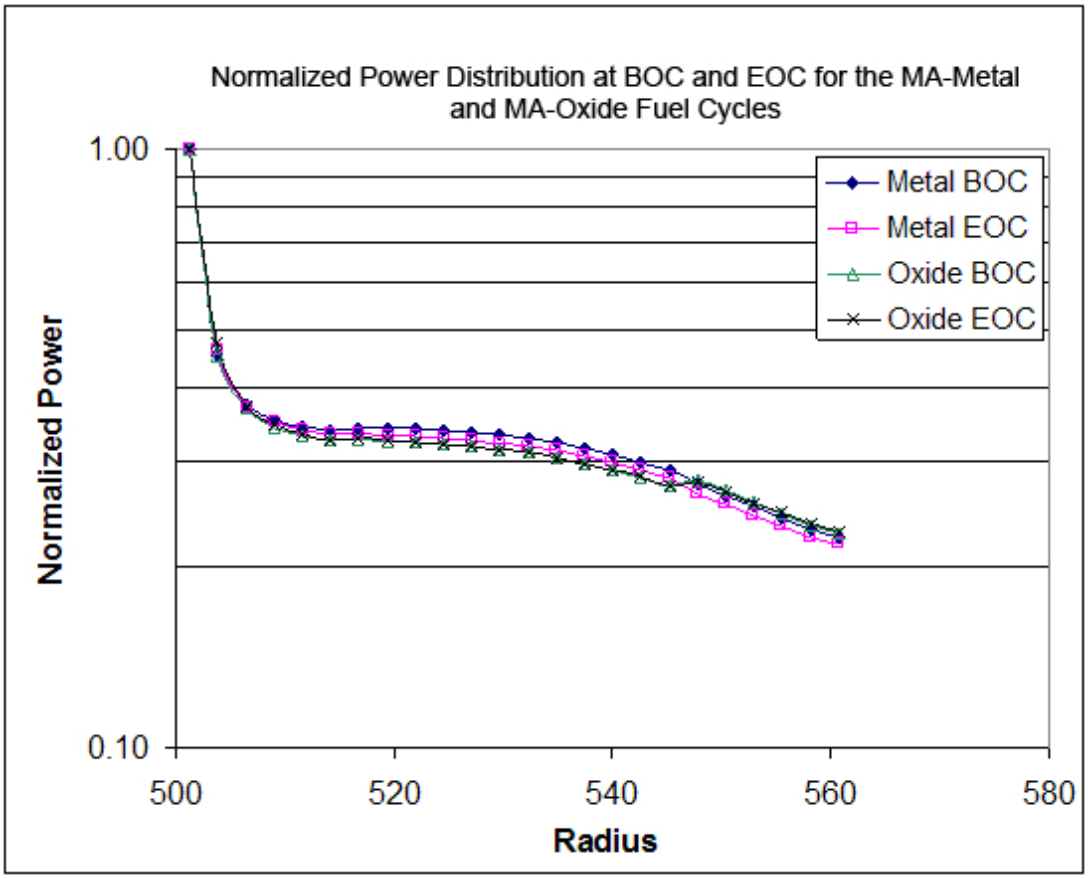

Figure 35: Radial Power Distributions for MA-Metal and MA-Oxide Fuel Cycles

The large power spike in the innermost assembly is caused by its location being next to the fusion neutron source, so there is an abundance of excess neutrons in the innermost fuel ring. The spectrum in the innermost fuel ring contains more low energy neutrons than in the outer fuel rings. This is seen in the Figures Neutron

Spectra by Ring for the MA-Oxide Fuel Cycle and Neutron Spectra by Ring for the MA-Metal Fuel Cycle. The greater number of low energy neutrons in the innermost ring is caused by neutrons hitting the inner tritium breeding blanket and reflecting back into the core. These low energy neutrons cause the large power peak near the first wall just as in the TRU burner. Figure 36 shows the power generated at BOC and EOC in each fuel region.

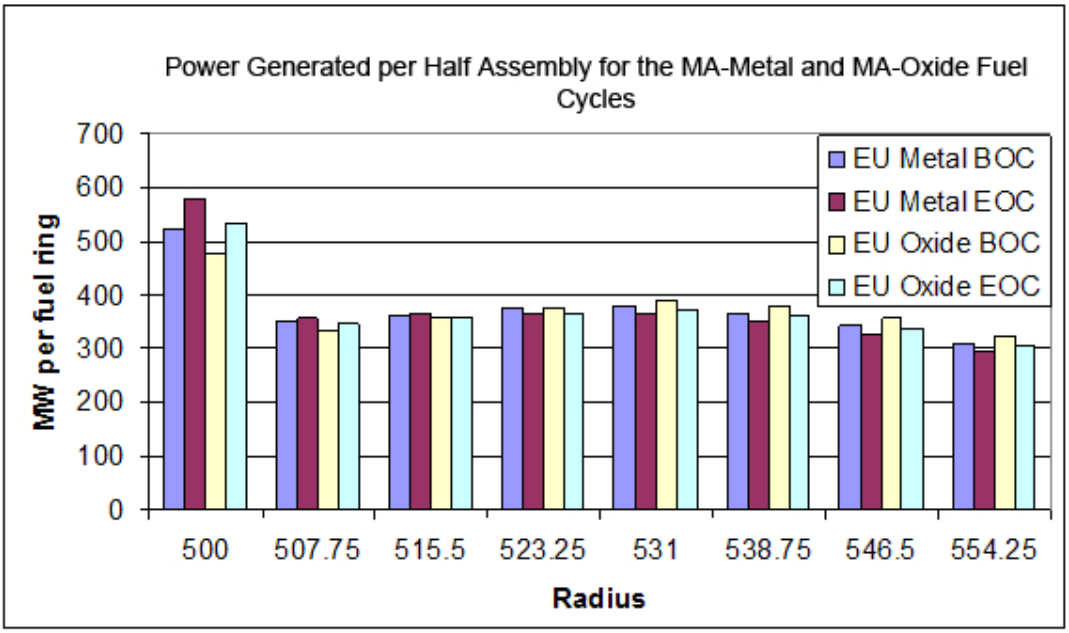

Figure 36: Power per Half Assembly for MA-Metal and MA-Oxide Fuel Cycles

The axial power profile for the MA burner is similar to that of a critical system. The profile is a cosine shape with two large peaks at the top and bottom. The peaks are caused by slower neutrons entering the system through the tritium breeding blankets as well as those being reflected back into the system by the breeding blankets. The axial power profile as a function of space for both the MA-Oxide and MA-Metal fuel is shown in Figures 37 and 38 below.

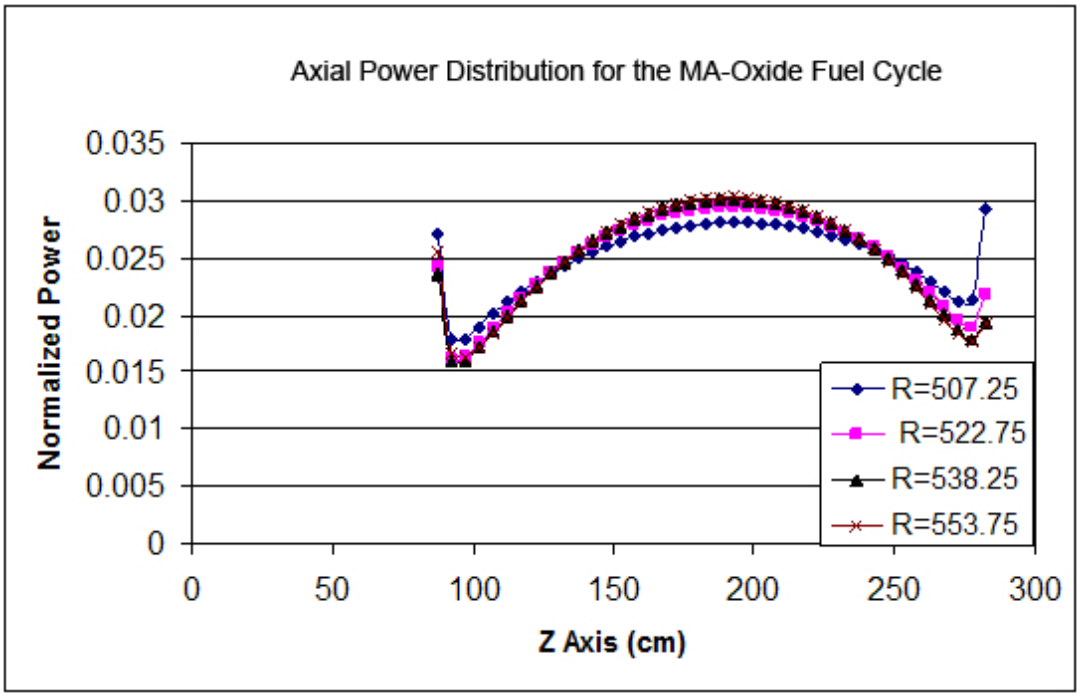

Figure 37: Axial Power Profile for the MA-Oxide Fuel Cycle

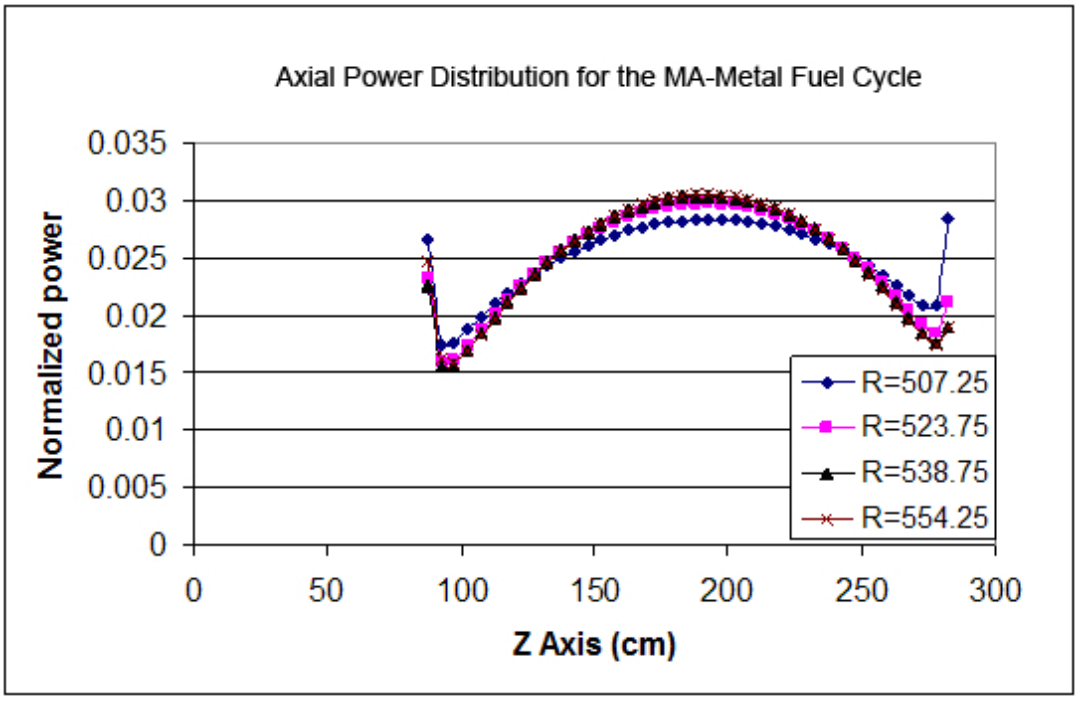

Figure 38: Axial Power Profile for the MA-Metal Fuel Cycle

The power peaks at the top and bottom of the reactor are caused by neutrons that have been reflected back into the system by the lithium orthosilicate breeding blanket. The power spike is slightly larger at the top of the core than the bottom of the core. This is because there are more neutrons at the top of the core than at the bottom from the fusion neutron source.

5.3.3 Repository Effects of the Metallic and Oxide Minor Actinide Burning Fuel Cycle

The EFIT fuel is designed with the transmutation strategy of "42-0", referring to the ratio of minor actinides burned to net plutonium burned 42 kg per terawatt hour for the minor actinides and zero kgs of plutonium. In SABR the EFIT fuel does not maintain the burning strategy of "42-0". It burns more plutonium than in the EFIT system. This is caused by the longer fuel irradiation times in SABR, 2800 days compared to 1095 days for EFIT. At the end of cycle the fuel that is being burned is no longer minor actinides but plutonium. The fuel does burn considerably more minor actinides than the TRU burning fuel; the oxide case burns approximately 1.9 times as many minor actinides per full power year, and the metallic case burns 2.4 times the amount of minor actinides per full power year. In the oxide fueled system 1.43 kilograms of minor actinides are destroyed for every one kilogram of plutonium that is burned, for the metallic fuel that ratio increases to 3.61 kilograms of minor actinides destroyed to every one kilogram of plutonium. Tables 15 and 16 show the BOC and EOC fuel composition as well as the fuel to the repository and back to fuel fabrication.

Table 15: SABR Fuel Compositions at BOC and EOC for the MA Burning Fuel Cycles (weight percent)

Isotope	MA-Oxide BOC	MA-Oxide EOC	MA-Metal BOC	MA-Metal EOC
U235	0.008	0.016	0.007	0.013
U238	4.401e-5	6.786e-5	4.440e-5	6.421e-5
Np237	2.014	1.908	2.010	1.931
Np239	6.348e-6	6.278e-6	6.438e-6	6.288e-5
Pu238	5.935	8.307	5.678	7.591
Pu239	17.638	15.651	17.434	15.766
Pu240	16.181	16.302	15.836	15.916
Pu241	2.010	2.170	1.897	2.020
Pu242	6.447	6.935	6.296	6.692
Am241	34.252	30.391	34.012	30.855
Am242m	0.941	1.218	0.802	1.055
Am243	7.821	7.294	7.736	7.308
Cm242	0.877	0.871	0.807	0.833
Cm243	0.072	0.096	0.063	0.082
Cm244	2.610	3.042	2.467	2.809
Cm245	0.645	0.685	0.619	0.646
Cm246	0.051	0.052	0.050	0.051
Cm247	0.001	0.001	0.001	0.001
Fission Products	2.357	4.813	4.144	6.211

Table 16: SABR Content to the Repository and Fuel Fabrication for the MA burning Fuel Cycles (kg)

Isotope	MA-Oxide Repository	MA-Oxide Fuel Fabrication	MA-Metal Repository	MA-Metal Fuel Fabrication
U235	0.026	2.612	0.023	2.271
U238	8.473e-5	0.008	8.695e-5	0.009
Np237	1.878	186.011	2.112	209.049
Np239	6.275e-6	6.21e-4	6.923e-6	0.001
Pu238	10.903	1079.369	10.617	1051.078
Pu239	14.535	1438.974	16.321	1615.802
Pu240	17.375	1720.101	18.498	1831.394
Pu241	2.713	268.572	2.691	266.419
Pu242	7.925	784.575	8.249	816.641
Am241	28.437	2815.262	32.241	3191.904
Am242m	1.439	142.422	1.410	139.57
Am243	7.237	719.424	8.023	794.300
Cm242	1.382	136.825	1.464	144.950
Cm243	0.147	14.642	0.133	13.119
Cm244	3.677	364.070	3.654	361.727
Cm245	0.832	82.399	0.828	81.99
Cm246	0.057	5.649	0.061	60.16
Cm247	0.001	0.106	0.001	0.135
Total TRU	98.917	9792.772	106.637	10557.090
Fission Products	959.453	9.691	928.342	9.377

The light water reactor support ratio for the MA burner fuel cycle is defined as the ratio of minor actinides burned in SABR to the amount of minor actinides produced in a 1000 MW_e light water reactor, typically about 25 kg of minor actinides per year [13]. The new definition of support ratio is required for this system because the goal is not to burn plutonium but save the plutonium for recycle in either future fast reactors or mixed oxide systems. The LWR support ratios for the SABR metallic and oxide Europeans fuels, assuming 75% availability, are 25.6 and 20.2 respectively.

The decay heat to the repository in this system is very similar for both the oxide and metallic fuels; the overall burnup is 17.1% and 15.5% respectively. This leads to 53.5 kilograms per year deposited in the repository for the oxide fueled system, and 57.5 kilograms per year for the metallic fueled system. The amount of fission products to the repository and the decay heat produced is quite similar in both instances. The amount of fission products is set by the power produced in the reactor and the fuels residence time which is the same in both cases, the decay heat produced by the fission products is determined by which fission products are produced in the system. The fission product production is based on what isotopes fission and the spectrum in which they fission. The neutron spectrum is very similar in both systems with the metal fueled system having a slightly harder spectrum, while the isotopes that are fissioned are essentially the same with a few more minor actinides and less plutonium being fissioned in the metallic system. The increase in effective repository space as compared to a light water reactor is 7.91 for the oxide system and 8.09 for the metallic system. Figure 39 shows the decay heat to the repository for the both the MA-Oxide and MA-Metal fuel as well as the discharge from a representative light water reactor.

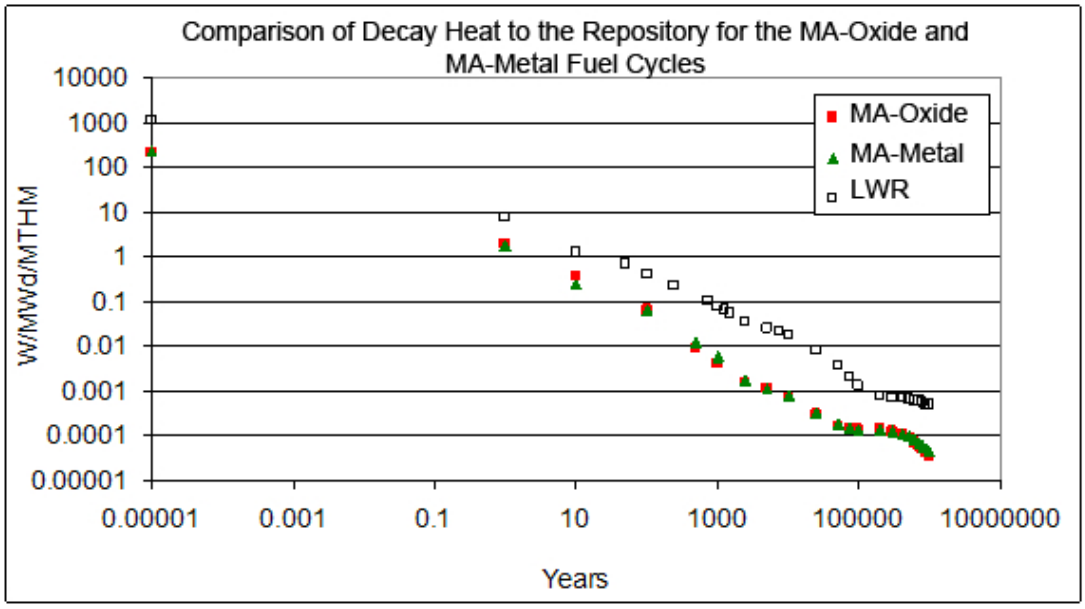

Figure 39: Decay Heat to the Repository MA-Oxide and MA-Metal Fuel Cycles

5.3.4 Tritium Breeding in the Metallic and Oxide Minor Actinide Burning Fuel Cycles

The tritium breeding ratio in both the MA oxide and metallic fuels is over 1 but less than 1.1. The oxide fuel has a slightly lower TBR because the production is similar in both cases but with the higher fusion power required to drive the system at 3000 MW_{th} in the fission core, a lower TBR results. Table 17 displays the tritium production and destruction rates as well as the TBR for both minor actinide burning fuels.

Table 17: Tritium Production for the MA Burning Fuel Cycles

	MA-Metal	MA-Oxide
BOC Tritium Destruction (atoms/sec)	6.74e19	6.95e19
BOC Tritium Production (atoms/sec)	1.03e20	1.04e20
EOC Tritium Destruction (atoms/sec)	8.72e19	1.15e20
EOC Tritium Production (atoms/sec)	1.38e20	1.52e20
Tritium Necessary for BOC (atoms)	6.18e21	6.52e21
Tritium at BOC (atoms)	6.66e21	6.54e21

The rest of the evaluation criteria: power peaking, radiation damage, and overall transuranic destruction rate for the metallic and oxide fuels in the minor actinide burning cycle were all very similar throughout the fuel cycle. This is a result of the fuels having similar BOL, BOC, and EOC reactivities and fusion powers. The oxide fuel performs better in terms of power peaking and overall burnup, 17.1% to 15.5% for the oxide and metallic fuel respectively.

5.4 SABR Fuel Cycle Comparisons

Two general fuel cycles were considered in the SABR reactor. The first fuel cycle considered was a transuranic burning fuel cycle in which all of the transuranics produced by the current light water reactor fleet are burned. The second fuel cycle was the minor actinide burning fuel cycle where all of the minor actinides and some of the plutonium produced in light water reactors are burned in SABR, while some of the plutonium is stored for setting up future fast reactor systems. This second fuel cycle is being considered in the European scenario studies [26], where EFIT and low conversion ratio fast reactors (LCRFR) have been studied.

The three fuel cycles were compared based on their transmutation performance.

To compare the transmutation performance the transmutation data per kg of initial heavy metal was examined. The data examined for the equilibrium fuel cycles are shown in Table 18.

When comparing the MA Burning SABR fuel cycles to both an LCRFR and the EFIT system, the systems are compared on their transmutation performance. The calculations done in the references by Romanello were used for the LCRFR and the EFIT system [26, 25, 27]. Table 19 illustrates the transmutation performance of each of the three systems.

Table 18: System Data for SABR Equilibrium Fuel Cycle

Cycle	TRU Burner		MA-Oxide		MA-Metal	
	Input	Output	Input	Output	Input	Output
TRU (g/MTIHM)	998338	852420	997455	906872	997216	906732
Plutonium (g/MTIHM)	743249	656184	513472	485946	520216	491730
Neptunium (g/MTIHM)	85327	51071	19863	18201	19510	17285
Americium (g/MTIHM)	88657	83634	402687	359277	403617	341758
Curium (g/MTIHM)	33054	36117	51067	52931	54111	56099
Pu238 (g/MTIHM)	126234	150086	75032	91513	88279	100301
Pu239 (g/MTIHM)	217086	123476	169476	140682	161494	133717
Pu240 (g/MTIHM)	62204	249299	171689	159452	171239	159841
Pu241 (g/MTIHM)	69473	56798	26017	23196	25111	24957
Am241 (g/MTIHM)	83160	53414	286721	277907	274085	272907
Fission Products (g/MTIHM)	14097	151448	789	80827	752	89157
Total TRU (kg)	7887	5845	12345	10234	13040	11013
Reprocessed Feed Rate	3048 (kg/yr)		5336 (kg/yr)		5742 (kg/yr)	
Makeup TRU Feed Rate	1065 (kg/yr)		1101 (kg/yr)		1057 (kg/yr)	

5.4.1 TRU Burning Fuel Cycle

The TRU burning core reprocess approximately 3,050 kg of transuranics per year. Utilizing the 1% reprocessing efficiency approximately 31 kg of transuranics per year are sent to geological repository and and 3,019 are sent to the fuel fabrication facitily

Table 19: Transmutation Capabilities of SABR, EFIT, and LCRFR

Cycle	SABR TRU Burner	SABR MA-Oxide	SABR MA-Metal	EFIT	LCRFR
Fuel Type	TRU-Zr	(TRU) O_2-Mg0	TRU MgO	(TRU) O_2-MgO	(U-TRU) O_2
MA/Pu Ratio	≈0.5	≈1.2	≈1.2	≈1.2	≈1.2
Fission Power (MW)	3000	3000	3000	384	1000
TRU Burned (kg/yr)	1027	1122	1089	141	262
Pu Burned (kg/yr)	685	469	236	6	1
MA Burned (kg/yr)	342	674	853	135	261
LWR Support Ratio	4.2[a]	27.0[b]	34.1[b]	5.4[b]	10.5[b]
Discharge Burnup %	25.6	17.1	15.5	10.7	13.2
Fuel Residence Time (days)	2800	2800	2800	1095	2100
Cycle Length (days)	700	700	700	365	326
Units to Transmute U.S. TRU/MA Production	24[c]	4[d]	3[d]	19[d]	10[d]

[a] Defined by the ratio of TRU destroyed in SABR to the amount of TRU produced in a 1000 MW_e LWR.

[b] Defined by the ratio of MA destroyed to the amount of MA produced in a 1000 MW_e LWR.

[c] Units to transmute United States transuranic production.

[d] Units to transmute United States minor actinide production.

and mixed with the fresh transuranics from light water reactors and placed back into the SABR core. The fewer kilograms of fuel to reprocessing in the TRU burner is caused by the different isotopic compositions in the core. The TRU burner fuel also has a higher percentage of matrix in the fuel 40% by weight as compared to 13% to 15% for the MA burning cores. This results in a smaller initial loading of transuranics and with the same transmutation rate less transuranics out of the system and to reprocessing and eventually the repository.

The TRU burning fuel cycle employed by SABR is capable of transmuting aproximately 1,050 kg of transuranics per year. Light water reactors in the United States currently approximately 25 MT of transuranics per year [13]. To transmute all of the transuranics produced in the United States per would require 24 TRU burning SABRs.

The 25 MT of transuranics per year produced in the United States are currently stored on reactor sites and the current plan is for geological disposal. The 24 TRU burning SABR systems required to burn these 25 MT or transuranics produced per year would reduce the amount of transuranics to the repository to 1,400 kilograms per year. The TRU burning SABR system reduces the amount of transuranics to the repository over the current once through fuel cycle by approximately a factor of 17.

5.4.2 Comparison of SABR Minor Actinide Burning Fuel Cycles to EFIT and LCRFR Fuel Cycles

The MA-Oxide and MA-Metal burning cores reprocess approximately 5,300 and 5,700 kg of transuranics per year respectively. The MA-Oxide fuel cycle sends 53 kilograms of transuranics per year to the repository, while the MA-Metal fuel cycle sends approximately 57 kilograms to the repository. These numbers do not include the transuranics produced by the plutonium that is transmuted in either mixed oxide systems or future fast reactor systems. The repository effects in this study do not consider the transuranics produced from fissioning of the saved plutonium in future

reactor systems.

The current light water reactor fleet in the United States produces approximately 2,500 kilograms of minor actinides per year. To transmute all of the minor actinides currently produced in the United States per year would take 4 SABR MA-Oxide burner reactors or 3 SABR MA-Metal burner reactors. Similary, to transmute all of the minor actinides produced using the LCRFR would necessitate ten reactor systems. If the EFIT system was chosen, 19 EFITs would be required to transmute all of the minor actinides produced by the current fleet of light water reactors. The SABR system is approximately 3 times more effective than the LCRFR and 5 times more effective than EFIT. The advantage over the LCRFR is two fold: first SABR utilizes a 100% transuranic fuel which results in a greater net transmutation rate and second SABR has a larger fission power resulting in a larger transmutation rate. The larger fission power utilized in SABR is the reason less SABR systems are required as compared to EFIT.

In transmuting all of the minor actinides produced by light water reactors in the United States, operating SABR with the MA-Oxide fuel results in 392 kilograms to the repository. Operating SABR with the MA-Metal fuel results in 320 kilograms of transuranics to the repository. If the LCRFR was chosen as the transmutation reactor there would be 1,350 kilograms of TRU to the repository, and if the EFIT system was chosen 2,550 kilograms to the repository. The higher burnup that is achievable in SABR is an advantage over both the LCRFR and the EFIT system. The MA-Oxide core obtains an average discharge burnup of 17.1% while the MA-Metal core obtains a discharge burnup of 15.5%. The discharge burnup is 2% to 4% higher in SABR than in the LCRFR and 5% to 7% higher than in EFIT.

CHAPTER VI

CONCLUSIONS

Two types of fuel cycles for a subcritical advanced burner reactor (SABR) consisting of an annular, Na-cooled fast reactor surrounding a tokamak fusion neutron source have been investigated. Each fuel cycle has inherit advantages and disadvantages associated with it. The first fuel cycle type was one in which all of the transuranics in spent nuclear fuel from a once through light water reactor fuel cycle are transmuted in SABR. This fuel cycle can be operated in a stand alone fashion and ultimately destroy greater than 90% of all of the transuranics from LWR spent nuclear fuel. This system does not differentiate between the plutonium and minor actinides in the spent light water reactor fuel. The second fuel cycle type is one in which some of the plutonium in LWR spent fuel is set aside for future use and the remaining plutonium plus the minor actinides are transmuted in SABR. To destroy greater than 90% of the transuranics from light water reactor spent fuel this system would need to be supplemented by either a fast reactor or a mixed oxide light water reactor for transmutation of the left over plutonium. However, this system does allow for the possibility of using the plutonium for future breeder reactors and increasing the energy utilization of the initial uranium fuel.

The accumulated radiation damage versus burnup for the Metal-TRU fuel was investigated. It was determined that there was not a large advantage in increasing the radiation damage limits beyond 200 dpa, both fuel cycle types set the fuel residence time between reprocessing steps by this radiation damage limit. The separation of transuranics from fission products was assumed to be only 99% efficient. It was discovered that by repeated recycling of the TRU burning fuel discharged from SABR

with a blend of "fresh" transuranics discharged from LWRs, the requirements for high level waste repositories could be reduced by a factor of about 10 relative to the repository requirements over just burying the discharged fuel from LWRs. This result is based on the conservative assumption that the actinide-fission product separation efficiency is only 99%. Increasing the actinide-fission product separation efficiency would reduce the amount of actinides that go to the high level waste repository; thus creating a greater reduction in the repository requirements.

The TRU burning core as well as the Minor Actinide burning cores experienced large power spikes in the inner most region of the fission core. These are caused by fusion neutrons being reflected off of the inner tritium breeding blanket and being slowed down to thermal energies before they entered the fission core. One method to reduce the power spike is to remove the inner tritium blanket; which would reduce the power generated in the first two centimeters of the core from 14% of the total power to 8% of the total power. Future investigations would need to be done to determine the loss of tritium breeding in the system from removal of the inner breeding blanket.

The minor actinide burning fuels that were used in SABR were designed for an accelerator driven system. These fuels were designed to have a minimal reactivity swing throughout the fuel cycle and were optimized for the EFIT system. The fuels can be modified such that they act as a pure burner system and lose reactivity throughout the entire cycle. From BOL to BOC, the EFIT fuel gains 5379 pcm for the metal fuel and 5735 pcm for the oxide fuel. At BOL the fusion power is much higher than at BOC and EOC and in the oxide fueled case is greater than 500 MW.

A larger coolant to volume ratio in the MA-Oxide fuel as compared to the MA-Metallic fuel, led to a softer neutron spectrum in the system; and thus a greater percentage of plutonium burned as compared to minor actinides. This influences the LWR support ratio in the minor actinide fueled SABR greatly resulting in the metallic fueled system to outperform the oxide system in terms of support ratio by a factor of

1.25. The softer spectra in the oxide fuel also resulted in the system having a lower overall power peaking and the reflected neutrons not having as large of an influence on the power profile as the MA-Metal fuel or TRU burning systems.

All three fuel cycles out perform both the LCRFR and EFIT system in terms of transmutation performance. One residence time in SABR generates 50.4 TW_{hr} of thermal energy and results in 58.4, 102, and 110 kg of heavy metal to a geological repository for the TRU burner, MA-Oxide fuel, and MA-Metal fuel cycles respectively; as compared to 142 and 208 kg of heavy metal for the LCRFR and EFIT systems. The pure minor actinide burning system has a support ratio approximately 3 times greater than the LCRFR and 6 times greater than the EFIT system. It takes 3 MA-metal fueled SABRs or 4 MA-oxide fueled SABRs to transmute all of the minor actinides generated by the current fleet of United States light water reactors, compared to 10 LCRFRs and 19 EFIT systems. These additional LCRFRs and EFIT systems result in 4.2 and 7.9 times more transuranics to the repository for the LCRFR and EFIT systems. The minor actinide burning fuel cycles do not account for the transuranics that are generated with the plutonium that is stored for use in future systems.

In an overall fuel cycle evaluation other factors beyond the transmutation performance need to be taken into account. The proliferation effects of the fuel cycle and economics need to be considered as well. Electrochemical reprocessing was chosen to minimize the proliferation aspects of the transmutation fuel cycle. Economically, the advantage SABR has over critical or accelerator driven systems is that fewer SABR systems would be necessary to transmute all of the transuranics generated by light water reactors in the United States.

A 3000 MW_{th} SABR operating on such fuel cycles, with 75% availability would be capable of burning all of the transuranics discharged annually from 3 1000 MW_e light water reactors, or to burn all the minor actinides and some of the plutonium

discharged from 20-25 1000 MW_e light water reactors. Thus, one could envision a nuclear fleet with 75% of the energy produced by light water reactors and 25% of the energy produced by SABRs that burned all the transuranics discharged from the light water reactors. Alternatively, one could envision a nuclear fleet with 95% of the energy produced by light water reactors and 5% produced by SABRs that burned the minor actinides (primarily) and some of the plutonium discharged from light water reactors, while plutonium was accumulated to start up fast reactors.

REFERENCES

[1] "Pyrochemical separations in nuclear applications," 2004. A Status Report. Nuclear Energy Agency, Organisation for Econominc Co-operation and Development.

[2] "Global Nuclear Energy Partnership technology development plan," July 2007. http://www.inl.gov/technicalpublications/Documents/3738885.pdf.

[3] "Development of radiation resistant reactor core structural materials," January 2010. http://www.iaea.org/About/Policy/GC/GC51/GC51InfDocuments/English/gc51inf-3-att7_en.pdf.

[4] "Nuclear regulatory commission," May 2010. http://www.nrc.gov/reactors/new-reactors/new-licensing-files/.

[5] Artioli, C. and et. al., "Minor actinide transmutation in ads: The EFIT core design," in *Proceedings of Conference on the Physics of Reactors*, September 2008. Interlaken, Switzerland.

[6] Artioli, C. and Sarotto, M., "Design of the EFIT-MgO/Pb core and fuel assemblies," tech. rep., EUROTRANS WP1.5 Safety Meeting, Lyon, October 2006.

[7] Bodansky, D., "Reprocessing spent nuclear fuel," *Physics Today*, pp. 80–81, December 2006.

[8] Doriath, J. Y., Rieunier, J. M., and Rimpault, G., *ERANOS Manuel Des Methodes - Les Calculs D'Evolution*. CEA.

[9] Duderstadt, J. J. and Hamilton, L. J., *Nuclear Reactor Analysis*. New York: Wiley, 1976.

[10] Floyd, J. P. and et al., "Tokamak neutron source for a fast transmutation reactor," *Fusion Science and Technology*, vol. 52, p. 727, 2007.

[11] Gho, C. J. and Palmiotti, G., "Bistro: Bidimensional sn transport optimise, un programme bidimensionnel de transport sn aux differences finies note n1 definision des algorithmes pour la geometrie x-y." Technical Report.

[12] Goff, M., "Processing of spent nuclear fuel," 2008. Nuclear Regulatory Commission Seminar, Rockville, Maryland, USA.

[13] Goldner, F. and Versluis, R., "Transmutation capabilities of gen-iv reactors," in *Proceedings of Actinide and Fission Product Partitioning and Transmutation Ninth Information Exchange Meeting*, September 2006. Nimes, France.

[14] Holtkamp, N., "The status of the iter design," *Fusion Engineering and Design*, vol. 84, pp. 98–105, 2009.

[15] Laidler, J., "Gnep spent fuel processing; waste streams and disposition options," 2007. Nuclear Waste Technical Review Board, Washington, D.C.

[16] Laidler, J., "Promoting safe, secure, and peaceful growth of nucler energy," 2010. Project on Managing the Atom and Russian Research Center Kurchatov Institute.

[17] Macfarlane, R. E. and Muir, D., *The NJOY Nuclear Data Processing System, Version 99*. Los Alamos National Laboratory.

[18] MADDOX, J. W., "Fuel cycle optimization of a helium-cooled, sub-critical, fast transmutation of waste reactor with a fusion neutron source," Master's thesis, Georgia Institute of Technology, 2006.

[19] McCombie, C. and Isaacs, T., "The key role of the back-end in the nuclear fuel cycle," *Daedalus*, vol. Winter, pp. 32–43, 2010.

[20] MEYER, M. K. and et al, "Development and testing of metallic fuels with high minor actinide content," tech. rep., Argonne National Laboratory, Idaho Falls, Idaho, April 2006.

[21] Oak Ridge National Laboratory, *SCALE5.1: A Modular Code System for Performing Standardized Computer Analyses for Licensing Evaluation*.

[22] Regalbuto, M. C. and et. al, "Solvent extraction process development for partitioning and transmutation of spent fuel," in *Proceedings of Actinide and Fission Product Partitioning and Transmutation Eighth Information Exchange Meeting*, 2004. Las Vegas, Nevada, USA.

[23] Rimpault, G., "Algorithmic features of the ECCO cell code for treating heterogeneous reactor subassemblies," tech. rep., International Conference on Mathematics and Computations, Reactor Physics and Environmental Analyses, Portland, OR, May 1995.

[24] Rimpault, G. and et al., "The eranos data and code system for fast reactor analyses," in *Proceedings of the International Conference on the New Frontier of Nuclear Technology: Reactor Physics, Safety and High-Performance Computing, PHYSOR*, October 2002. Seoul, South Korea.

[25] Romanello, V. and et. al., "Advanced fuel cycle scenario study in the european context by using different burner reactor concepts," in *Proceedings of Actinide and Fission Product Partitioning and Transmutation Eleventh Information Exchange Meeting*, November 2010. San Francisco, California, USA.

[26] Romanello, V. and et al., "Comparative study of fast critical burner reactors and subcritical accelerator driven systems and the impact on transuranics inventory in a regional fuel cycle," *Nuclear Engineering and Design*, pp. 433–443, JANUARY 2011.

[27] Romanello, V. and et. al., "Comparison of the waste transmutation potential of different innovative dedicated systems and impact on the fuel cycle," in *Proceedings of the 16th International Conference on Emerging Nuclear Energy Systems*, MAY 2011. San Francisco, California, USA.

[28] Russel, J. and et. al., "Rethinking the challenge of high level nuclear waste: Strategic planning for defense high-level waste and spent fuel disposal," May 2007. `http://www.clarku.edu/mtafund/prodlib/yakama/Rethinking_the_Challenge_of_High-Level_Nuclear_Waste.pdf`.

[29] S. Hayes, M. M., 2007. personal communication.

[30] Salvatores, M. and Palmiotti, G., "Radioactive waste partitioning and transmutation within advanced fuel cycles : Achievments and challenges," *Progress in Partical and Nuclear Physics*, vol. 66, pp. 144–166, 2011.

[31] Smith, M. A., "Low conversion ratio fuel studies, ANL-AFCI-163," tech. rep., Argonne National Laboratory, Downers Grove, Illinois, January 2006.

[32] Sommer, C. M., "Fuel cycle design and analysis of sabr: Subcritical advanced burner reactor," Master's thesis, Georgia Institute of Technology, 2008.

[33] Sommer, C. M., Stacey, W. M., and Petrovic, B., "Fuel cycle analysis of the sabr subcritical transmutation reactor concept," *Nuclear Technology*, vol. 172, pp. 48–59, 2010.

[34] Stacey, W. M. and et. al., "A fusion transmutation of waste reactor," *Fusion Engineering and Design*, vol. 63, pp. 81–86, 2002.

[35] Stacey, W. M. and et. al., "A sub-critical, gas-cooled fast transmutation reactor (gcftr) with a fusion neutron source," *Nuclear Technology*, vol. 150, p. 162, 2005.

[36] Stacey, W. M. and et. al., "A sub-critical, he-cooled, fast reactor for the transmutation of spent nuclear fuel," *Nuclear Technology*, vol. 156, p. 99, 2006.

[37] Stacey, W. M. and et. al., "Advances in the sub-critical, gas-cooled, fast transmutation reactor concept," *Nuclear Technology*, vol. 159, p. 72, 2007.

[38] Stacey, W. M. and et. al., "A tru-zr metal fuel, sodium cooled, fast subcritical advanced burner reactor," *Nuclear Technology*, vol. 162, p. 53, 2008.

[39] Stacey, W. M. and et. al., "SABR fusion-fission hybrid fast burner reactor based on iter," in *Proceedings of Actinide and Fission Product Partitioning and Transmutation Eleventh Information Exchange Meeting*, November 2010. San Francisco, California, USA.

[40] Sublet, J. C., Ribon, P., and Coste-Delclaux, M., *CALENDF-2005 : User Manual*. CEA.